

1 The dynamic-thermal structures of the planetary boundary layer dominated by
2 synoptic circulations and the regular effect on air pollution in Beijing

3 Yunyan Jiang^{*1,2}, Jinyuan Xin^{**1,2,3}, Ying Wang⁴, Guiqian Tang¹, Yuxin Zhao^{3,5}, Danjie Jia^{1,2}, Dandan
4 Zhao^{1,2}, Meng Wang¹, Lindong Dai¹, Lili Wang¹, Tianxue Wen¹, Fangkun Wu¹

5
6 ¹ State Key Laboratory of Atmospheric Boundary Layer Physics and Atmospheric Chemistry (LAPC), Institute of
7 Atmospheric Physics, Chinese Academy of Sciences, Beijing 100029, China

8 ² University of Chinese Academy of Sciences, Beijing 100049, China

9 ³ Collaborative Innovation Center on Forecast and Evaluation of Meteorological Disasters, Nanjing University of
10 Information Science & Technology, Nanjing, 210044, China

11 ⁴ College of Atmospheric Sciences, Lanzhou University, Lanzhou 730000, China

12 ⁵ Institute of Atmospheric Composition, Chinese Academy of Meteorological Science, Beijing 100081, China

13
14 * These authors contributed equally to this work.

15 * Correspondence: Jinyuan Xin; email: xjy@mail.iap.ac.cn; phone: (+86)010-62059568; address: #40 Huayanli,
16 Chaoyang District, Beijing 100029, China

17 **Abstract.** To investigate the impacts of multiscale circulations on the planetary boundary layer (PBL), we have
18 carried out the PBL dynamic-thermal structure field experiment with a Doppler Wind Profile Lidar, a microwave
19 radiometer and a ceilometer from January 2018 to December 2019 in Beijing. We found that the direct regulatory
20 effect of synoptic circulation played a leading role in the daytime by transporting and accumulating pollutants in
21 front of mountains. While the indirect effect of multiscale circulations played a leading role in the nighttime by
22 coupling mechanisms. The horizontal coupling of different direction winds produced a severe pollution
23 convergent zone. The vertical coupling of upper environmental winds and lower regional breezes regulated the
24 mixing and diffusion of pollutants by generating dynamic wind shear and advective temperature inversion. We
25 also found that the dominated synoptic circulations leaded to great differences in PBL dynamic-thermal structure
26 and pollution. The cyclonic circulation resulted in a typical multilayer PBL characterized by high vertical shear (600
27 m), temperature inversion (900 m) and an inhomogeneous stratification. Meanwhile, strong regional breezes
28 pushed the pollution convergent zone to the south of Beijing. The southwesterly circulation resulted in a
29 mono-layer PBL characterized by low vertical shear (400 m) and inversion (200 m). The westerly circulation leaded
30 to a hybrid-structure PBL, and the advective inversion generated by the vertical shear of zonal winds. Strong
31 environmental winds of southwesterly and westerly circulations pushed the severe pollution zone to the front of
32 mountains. There was no distinct PBL structure under the anticyclone circulation. The study systematically
33 revealed the appreciable effects of synoptic and regional circulations on PBL structure and air quality, which
34 enriched the prediction theory of atmospheric pollution in the complex terrain. Synoptic circulations play
35 important roles in meteorological conditions and air quality within the planetary boundary layer (PBL). Based on
36 Lamb-Jenkinson weather typing and multiple field measurements, this study reveals the mechanism of how the
37 coupling effects of multiscale circulations influence PBL structure and pollution. Due to the topographic blocking
38 in the daytime, pollutants accumulate in the plain areas horizontally. The sinking divergent flows overlying on the
39 rising convergent flows within the PBL inhibit the continuously upward dispersion of aerosols vertically. At night,
40 the horizontal and vertical coupling mechanisms synergistically worsen the pollution. The large scale
41 environmental winds and regional scale breezes affect the pollution directly via the horizontal coupling effect,

42 which generates a pollution convergent zone of different directional flows. The relative strength of flows causes
43 the severely polluted area to move around horizontally from 39°N to 41°N. In addition, the multiscale circulations
44 regulate the mixing and diffusion of pollutants indirectly via the vertical coupling effect, which changes the PBL
45 dynamic thermal structure. The warm advection transported by the upper environmental winds overlies the cold
46 advection transported by the lower regional breezes, generating strong wind direction shear and advective
47 inversion. The capping inversion and the convergent sinking motion within the PBL suppress massive pollutants
48 below the zero speed zone. The multilayer PBL under cyclonic circulation has no diurnal variation. Weak ambient
49 winds strengthen the mountain breezes observably at night, the temperature inversion can reach 900 m. The
50 nocturnal shallower PBL, consistent with the zero velocity zone between ambient and mountain winds, can reach
51 600 m. By contrast, the PBL under southwesterly circulation is a mono-layer with obvious diurnal variation,
52 reaching 2000 m in the daytime. The strong winds circulations restrain the development of regional breezes, the
53 zero speed zone is located at 400 m and the inversion is lower than 200 m at night. The PBL under westerly
54 circulation has a hybrid structure with both multiple aerosol layers and diurnal variation. The inversion is
55 generated by the vertical shear of zonal winds. Clean and strong north winds are dominated under anticyclone
56 circulation, the vertical shear and the diurnal variation of thermal field disappear because of strong turbulent
57 mixing, and there is no significant PBL structure. Our results imply that the algorithm of atmospheric
58 environmental capacity under synoptic circulations, such as the cyclonic type, with a multilayer PBL needs to be
59 improved.

60 **Keywords** Synoptic Circulation Types, Planetary Boundary Layer, Multiscale Circulations Coupling, Regional
61 Breezes, Air Pollution

62 1. Introduction

63 Beijing megacity is the political, economic and cultural center of China. With the recent economic
64 development and acceleration of urbanization, an increasing number of air pollution episodes have emerged and
65 pose a direct threat to human health (Quan et al., 2014; Fu et al., 2014; Cheng et al., 2016; Song et al., 2017).
66 Thus, numerous comprehensive observations and studies on the planetary boundary layer (PBL) and air pollution
67 have been carried out in recent years. Severe pollution is closely related to emissions (Zhang et al. 2012; Wang
68 and Chen 2016), synoptic circulations (Wang et al., 2014; Wu et al., 2017; Liao et al., 2017; Miao et al., 2017a, b),
69 topography (Wang et al., 2018; Zhang et al., 2018) and physical and chemical reaction processes (Sun et al., 2015;
70 Zheng et al., 2015a; Yang et al., 2016). In addition to local emissions in Beijing, massive pollutants are generated
71 in southern Hebei Province and transported northward to Beijing through regional transportation (Miao et al.,
72 2016; Chang et al., 2018; Han et al., 2018). Emissions in a particular area normally do not change much over a
73 short period; however, large-scale atmospheric circulations play a leading role in the transportation,
74 accumulation and dispersion of pollution and thus result in the day-to-day variation of air qualitypollutants (Tai et
75 al., 2010²⁰¹²; Zhang, 2017; Wang et al., 2018). Zheng et al. (2015b) explored the relationships between AOD and
76 synoptic circulations and found that a uniform surface pressure field in eastern China or a steady straight westerly
77 in the middle troposphere is typically responsible for heavy pollution events. Miao et al. (2017a) specially
78 targeted summertime synoptic types, indicating that the horizontal transport of pollutants induced by the
79 synoptic forcing is the most important factor affecting the air quality of Beijing in summer. They also found that
80 synoptic patterns with high-pressure systems located to the east or southeast of Beijing are the most favorable
81 types for heavy aerosol pollution events. Li et al. (2020) quantitatively analyzed the contributions of different
82 large-scale circulations toPM2.5. Many approaches have been used to classify the synoptic circulations, which
83 can be mainly divided into subjective and objective methods. Objective weather typing methods have the
84 advantages of convenient operation, high objectivity and efficiency, hence they have been employed widely in

85 recent years (Zhang et al., 2016; Ye et al., 2016; Miao et al., 2017a). In this study, we adopt an objective
86 Lamb-Jenkinson classification scheme to categorize the large-scale atmospheric circulations centered on Beijing.
87 The Lamb-Jenkinson approach, which is confirmed that the categorization results have clear physical
88 understanding, has been applied widely in previous studies (Huang et al., 2016; Liao et al., 2017; Yu et al., 2017).

89 In addition, Beijing is located in the North China Plain (NCP) region and is-surrounded by Yan and Taihang
90 Mountains to the north and west, respectively (Fig. 1b). The Bohai Sea lies to the southeast and is approximately
91 150 km from Beijing. This semibasin topography blocks and decelerates the relatively weak southerly airflows (Li
92 et al., 2007). Aerosol pollutants from southern provinces through regional transportation stagnate and converge
93 in front of the mountains, leading to the accumulation zone of pollution. In addition, Bohai Sea lies to the
94 southeast and is approximately 150 km from Beijing. This unique geographic location and topography results in
95 diurnal variations in the mountain-plain breeze (MPB) and sea-land breeze (SLB) under relative weak synoptic
96 circulationsflows. The SLB can penetrate deep into the mainland when it is blooming, and aerosol pollution
97 transported previously over the sea could be recirculated to the Beijing-Tianjin-Hebei region (Liu et al., 2009;
98 Miao et al., 2017a; Bei et al., 2018). As Beijing is surrounded by mountains and relatively far from the Bohai Sea,
99 the intensity of the MPB circulation is much stronger compared to the sea-land breeze circulation in Beijing (Chen
100 et al., 2009; Miao et al., 2015a, b), especially when synoptic circulations dominate in Bohai areas. Miao et al.
101 (2015b) found that the regional-scale MPB circulations can modulate aerosol pollution by lifting or suppressing
102 PBL. Chen et al. (2009) found that the MPB played an important role in the vertical transportation and dispersion
103 of pollutants via the mountain chimney effect.

104 The PBL structure is also a key factor affecting the distribution and intensity of pollutants in addition to the
105 circulations. The thermal structure of the PBL determines the vertical dispersion of aerosols. In the daytime
106 convective layer, air pollution tends to be mixed vertically and homogeneously because of intensified turbulence
107 and eddies of different sizes by radiation (Stull, 1988). After sunset, the turbulence decays and a stable boundary
108 layer forms with weak turbulence. A radiation inversion on the ground caps the pollutants and leads to the
109 accumulation near the surface. Hu et al. (2014) found that westerly warm advection above the Loess Plateau was
110 transported over the NCP and imposed a thermal inversion, which acted as a lid and capped the pollution in the
111 boundary layer (Xu et al., 2019). The dynamic structure of the PBL, including wind shears and turbulence, can
112 modify air quality by influencing the dispersion and transport processes of air pollutants (Li et al., 2019). Zhang et
113 al. (2020) found that a much weaker vertical wind shear was observed in the lower part of the PBL under polluted
114 conditions, compared with that under clean conditions, which could be caused by the strong ground-level PM2.5
115 accumulation induced by weak vertical mixing in the PBL. In turn, the particulate matter can also affect the PBL
116 structure by scattering and absorbing of solar radiation, and lead to severe pollution by positive feedback (Petaja
117 et al., 2016; Li et al., 2017). Ding et al. (2016) suggested that black carbon enhanced haze pollution in megacities in
118 China by heating upper PBL and cooling surface. Lou et al. (2019) investigated the relationships between PBL
119 height and PM2.5 and indicated that the strongest anticorrelation occurred in the NCP region at 1400 Beijing
120 time. However, due to the lack of comprehensive observation with high vertical resolution, the dynamic and
121 thermal PBL structure, as well as the mechanisms of how the synoptic circulations and regional scale circulations
122 influence the PBL structure and air quality, is not well understood. Therefore, the relationships among the
123 multiscale circulations, PBL structure and air pollution should be studied in depth. Many classification approaches
124 have been used to discuss the distinctions of different synoptic circulations, which can be mainly divided into
125 subjective and objective methods. Objective weather classification methods have the advantages of convenient
126 operation, high objectivity and efficiency, hence they have been employed widely in recent years (Zhang et al.,
127 2016; Ye et al., 2016; Miao et al., 2017a). In this study, we adopt an objective Lamb-Jenkinson classification
128 scheme to categorize the large-scale atmospheric circulations centered on Beijing. The Lamb-Jenkinson approach

129 has been applied in many previous studies (Huang et al., 2016; Liao et al., 2017; Yu et al., 2017), which have
130 confirmed that the categorization results have clear physical understanding.

131 This study is based on different synoptic circulations and attempts to investigate the synergetic effects of
132 multiscale circulations on the PBL dynamic thermal structure and air pollution in detail. To sum up, because of
133 the unique topography and geographic location of Beijing, large-scale circulation and regional-scale
134 thermodynamic circulation both have appreciable impacts on PBL and air pollution. What are the characteristics
135 of PBL structure and the temporal and spatial distribution of pollution under different circulation types, and how
136 do the multiscale circulations jointly force the PBL structure to change when they coexist are still unrevealed.
137 Therefore, one objective of this study is to investigate the PBL dynamic-thermal structure and the distribution of
138 severe pollution area under the most frequent circulation types in Beijing. The other primary objective is to
139 further explore the synergetic effects of multiscale circulations on PBL and pollution in detail. Since the weather
140 typing approach is able to classify the synoptic circulations into different types and the high vertical resolution
141 remote sensing observations can measure the fine dynamic-thermal structures of PBL, the objectives can be
142 achieved by employing weather typing approach and remote sensing measurements as a necessary first step. The
143 remainder of this paper is organized as follows. Sect. 2 describes the instruments, data and method. Sect. 3
144 classifies the synoptic circulation types and selects typical types as research objects. Moreover, it further
145 investigates how the coupling mechanism of synoptic circulations and regional-scale circulations changes the
146 dynamic and thermal PBL structure and air pollution. Sect. 4 discusses the improvements on previous studies and
147 summarizes the main findings primary conclusions.

148 2. Data and Method

149 A PBL field observation experiment was performed from January 2018 to December 2019 basing on
150 multiple remote sensing devices, including Doppler Wind Profile Lidar, microwave radiometer (MWR) and
151 ceilometer in the courtyard of the Institute of Atmospheric Physics (39.6°N and 116.2°E), Chinese Academy of
152 Sciences, Beijing (Fig. 1b). We systematically probed the PBL dynamic structure, thermodynamic structure and the
153 vertical distribution of aerosols using the Lidar three-dimensional winds, the MWR temperature and humidity
154 profiles and the ceilometer backscattering coefficient respectively. The original remote sensing data, with high
155 temporal and spatial resolution, are fully capable to show the fine PBL dynamic-thermal structure. The reanalysis
156 data of mean sea level pressure (MSLP) and winds are used to depict the synoptic circulations, and winds from
157 hundreds of automatic weather stations to characterize the fine regional circulations. Thus, the synergistic
158 impacts of coexisting synoptic-scale and regional-scale circulations on the PBL dynamic-thermal structure and air
159 pollution in Beijing megacity can be well understood using the remote sensing and meteorological data in
160 combination with the Lamb-Jenkinson weather typing approach. The typical cases lasting two days in the same
161 weather type (C, SW, W and A) are on October 22 to 24, July 26 to 28, May 15 to 17 in 2019 and December 28 to
162 30 in 2018 respectively. Due to the algorithm limitations on the observation conditions, the data of backscattering
163 coefficient and temperature profiles are missing about 5 hours on July 27, 2019. it the remote sensing and
164 meteorological data

165 2.1 Meteorological data

166 The daily mean sea level pressure (MSLP) and wind fields at 850 hPa were obtained from the National
167 Center for Atmospheric Research (NCAR) reanalysis data (gridded at $2.5^\circ \times 2.5^\circ$). The divergence and vertical
168 velocity reanalysis data, with a horizontal resolution of $1^\circ \times 1^\circ$ and a temporal resolution of 1 h, were obtained
169 from Re-analysis Interim (ERA Interim) of European Centre for Medium-Range Weather Forecasts (ECMWF). The
170 hourly mean wind fields at the surface in the Beijing Tianjin Hebei area were collected by hundreds of automatic
171 weather stations operated observation data provided by the China Meteorological Administration (CMA).

172 **2.2-1** Remote sensing data

173 The high temporal and spatial resolution data of meteorological fields in the boundary layer are obtained by
174 multiple remote sensing devices are capable to show the fine PBL dynamic thermal structure. The measuring
175 location of ceilometer, Doppler Lidar and microwave radiometer (MWR) is 39.6°N and 116.2°E, in the courtyard of
176 the Institute of Atmospheric Physics, Chinese Academy of Sciences (Fig. 1b). Steyn et al. (1999) had shown that
177 the aerosol concentration in mixing layer (ML) is close to constant and significantly larger than that in the air
178 above. Thus, the ceilometer (CL31, Vaisala) BL-VIEW software derives the PBL height by BL-VIEW software
179 according to the minimum value of the local backscatter gradient (Tang et al., 2015), basing on the assumption
180 that the aerosol concentration in mixing layer (ML) is close to constant and significantly larger than that in the air
181 above (Steyn et al., 1999). The BL-VIEW algorithm excluded profiles with fog, precipitation or low clouds,
182 therefore resulting in the missing value of attenuated backscatter coefficient on July 27, 2019 used in
183 southwesterly circulation. The vertical resolution of the backscatter is 10 meters and the maximal detection
184 range can reach 7.7 km. A full overlap is achieved by using the same telescope for transmitting and receiving so
185 that the backscatter can be used from the first range gate (Münkel et al., 2007). This gives a clear advantage over
186 other commonly used Automatic Lidars and Ceilometers that usually show great uncertainty in the range below
187 200–500 m (Kotthaus et al., 2018). Three possible PBL heights, with a temporal resolution of 10 minutes, can be
188 output simultaneously to characterize the multiple aerosol layers structure according to the first three largest
189 negative gradients of backscatter. The typical uncertainty of CL31 on attenuated backscatter coefficient is $\pm 20\%$
190 and is ± 200 m on PBL height determination compared with radiosonde and other active remote sensors
191 (Tsaknakis et al., 2011). The intensity of backscatter are primarily determined by the concentrations of aerosol
192 particulates; hence, the PBL height derived from the BL-VIEW is a material PBL.

193 A Windcube 100S scanning Doppler Lidar is used to measures the wind profiles basing on the Doppler shift
194 of aerosol particulate backscatter signals using the light detection and ranging (Lidar) technique. Dai et al. (2020)
195 suggested that the Doppler Wind Profile Lidar is fully capable to measure three-dimensional winds by comparing
196 with cup anemometer and sonic wind anemometer. The vertical measuring range is from 50 m to 3.3 km. Several
197 scanning modes are available and the DBS (Doppler Beam Swinging technique) mode, which includes four LOS
198 (lines of sight) spaced 90° apart with a fixed elevation angle and one vertical LOS, is selected to detect the profiles
199 of winds. The vertical resolution of the profiles is 25 m and the temporal resolution is 20 s. The velocity
200 uncertainty along each LOS is associated with carrier-to-noise ratio (CNR) for each measurement volume following
201 the methodology from O'Connor et al. (2010). Typically, a threshold of -22 or -23 dB is used as a limit for the
202 accepted uncertainty in the Lidar measurements (Gryning et al., 2016), which corresponds to an uncertainty of
203 about 0.15 m s^{-1} (Aitken et al., 2012; Suomi et al., 2017).

204 The temperature and relative humidity profiles in RPG-HATPRO MWR are determined by neural network
205 (NN) algorithm, and the vertical resolution of the profiles is 10–30 m in the lowest 0.5 km, 40–90 m from 0.5 km
206 to 2.5 km, 100–200 m from 2 km to 10 km, and the temporal resolution is 1 s. The MWR used in this study has
207 been tested by comparing with radiosonde observations (Zhao et al., 2019). The systematic errors increase with
208 altitude, and the MWR-retrieved temperature and relative humidity are of quite high reliability inside the PBL.
209 The temperature biases and RMSEs are -2.0 °C and 1.2 °C under 2 km, and the minimum of biases and RMSEs are
210 between 1 km and 2 km, less than 0.5 °C and 1.3 °C respectively. Since the relative humidity derived from the
211 temperature and water vapor density, both the errors can cause the uncertainties. The bias and RMSE of relative
212 humidity is about -5% and 15% under 2 km. Furthermore, the residual liquid droplets on the water film led to
213 high brightness temperature measured by the MWR, resulting in the abnormal high values of the temperature
214 and humidity data. Therefore, data on July 27, 2019 were eliminated and substituted with missing values.

215 **2.2 Meteorological data**

216 The daily MSLP and wind at 850 hPa from the National Center for Atmospheric Research (NCAR) reanalysis
217 data (gridded at 2.5° × 2.5°) were used to classify the synoptic circulation patterns and depict the background
218 circulations of the typical circulation types. The divergence and vertical velocity reanalysis data (gridded at 1° × 1°)
219 with a temporal resolution of 1 h from Re-analysis Interim (ERA-Interim) of European Centre for Medium-Range
220 Weather Forecasts (ECMWF) were used to study the vertical motion in the mid-low troposphere in the NCP region
221 and its impact on PBL structure.. The hourly mean wind at the surface in the Beijing-Tianjin-Hebei area were
222 collected by hundreds of automatic weather stations operated by the China Meteorological Administration
223 (CMA).

224 2.3 Pollutant data

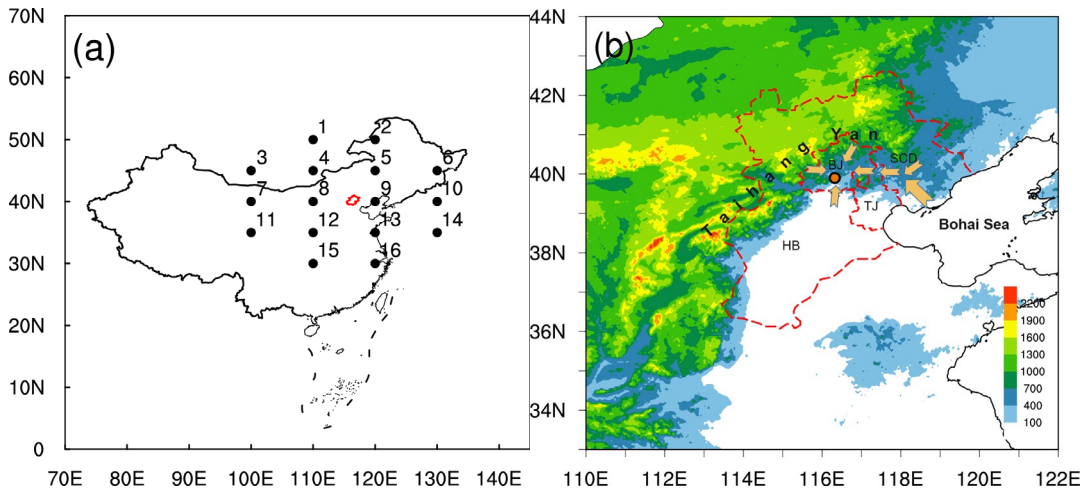
225 The hourly PM2.5 concentrations in the Beijing-Tianjin-Hebei monitoring sites are acquired from the
226 National Urban Air Quality Real-time Publishing Platform (<http://106.37.208.233:20035/>) issued by the Ministry of
227 Ecology and Environment. There are Beijing has 35 air quality monitoring stations in Beijing (Fig. 4a) and other
228 areas have 68 monitoring sites in Tianjin and Hebei provinces (Fig. 5, 7, 9) total. The PM2.5 concentration in
229 Beijing are shown in shaded by interpolating data of 35 sites, while the PM2.5 concentration in other areas are
230 shown in scatter with color as the spatial resolution is relative low. The PM2.5 data of Olympic Center station,
231 which is the closest monitoring site to the location of remote sensing measurements (less than 1 km), is used in
232 the circulation classification.

233 2.4 Method

234 The Lamb-Jenkinson weather typing (LWT) approach is widely adopted in large-scale circulation
235 classification (Lamb 1972; Jenkinson and Collison, 1977) because of its automation and explicit meteorologically
236 meaning. To classify the synoptic circulation types, the daily MSLP in 2018 and 2019 were used. The LWT scheme
237 is a half-objective categorization method. The weather patterns are predefined and each day can be identified
238 objectively as one certain type according to a small number of empirical rules (Trigo and DaCamara, 2000). As
239 shown in Fig. 1a, 16 gridded pressure data surrounding the study area (Beijing city) were selected to calculate the
240 direction and vorticity of geostrophic wind. The synoptic circulation can be classified into 26 types in total
241 including two vorticity types (cyclonic, C; anticyclonic, A), eight directional types (northeasterly, NE; easterly, E;
242 southeasterly, SE; southerly, S; southwesterly, SW; westerly, W; northwesterly, NW; and northerly, N), and sixteen
243 hybrid types (CN, CNE, CE, CSE, CS, CSW, CW, CNW, AN, ANE, AE, ASE, AS, ASW, AW, and ANW).

244 The gradient Richardson number (Ri) is the ratio of the buoyancy term to the shear term in the turbulent
245 kinetic equation. A negative Ri is an indication of buoyancy-generated turbulence, while positive Ri less than 0.25
246 indicates shear turbulence and dynamic instability. When Ri is larger than 0.25 and less than 1.0 the flows
247 become neutral, or exhibit hysteresis and still maintain turbulent. Otherwise, Ri larger than 1.0 means turbulent
248 flow will turn to be dynamically stable laminar (Stull, 1988). The distributional characteristics of Ri can reveal
249 whether the PBL has a stratified structure or not (Banakh et al., 2020). Thus, we adopt the critical values of 0.25
250 and 1.0 as a criterion to determine the PBL structure. It is able to estimate the atmospheric turbulent stability and
251 Ri can be calculated by Equation- 1, where g is the acceleration of gravity and Δz is the height interval between
252 adjacent layers. $\bar{\theta}$ is the mean virtual potential temperature, $\bar{\Delta u}$ and $\bar{\Delta v}$ is the mean zonal and
253 meridional wind speeds within the height interval respectively. Previous studies (Stull, 1988; Guo et al., 2016)
254 suggested that when Ri is smaller than the critical value (0.25), the laminar flow becomes unstable. Thus, we
255 adopt the value of 0.25 as a criterion to determine whether the layer is stable or not.

$$256 R_i = \frac{\frac{g}{\bar{\theta}} \frac{\Delta \bar{\theta}}{\Delta z}}{\left(\frac{\Delta \bar{u}}{\Delta z}\right)^2 + \left(\frac{\Delta \bar{v}}{\Delta z}\right)^2} \quad (1)$$



257
258 Fig. 1 The location of Beijing city in China (red lines). The and the locations of 16 black points show the location
259 of the $5^\circ \times 10^\circ$ MSLP grids data of the $5^\circ \times 10^\circ$ MSLP used for Lamb-Jenkinson weather type classification (black
260 dots) (a). The terrain height of the North China Plain (shaded, units: m). The filled dots show and the locations of
261 remote sensing devices (orange dot) (b). The arrows indicate the horizontal coupling mechanism of how
262 multiscale circulations affect pollution by generating convergent zone.

263 3. Results and Discussions

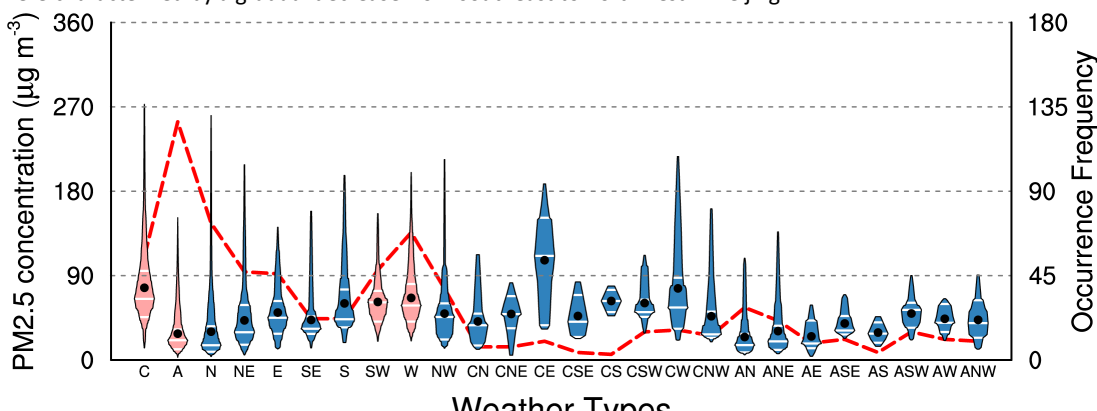
264 3.1 The typical weather types and PM2.5 distribution

265 Based on the Lamb-Jenkinson weather typing approach, synoptic circulations from 2018 to 2019 were
266 classified into predefined 26 circulation patterns and each day has a specific type. The distributional
267 characteristics of daily averaged PM2.5 concentration, as well as the occurrence frequency of different circulation
268 patterns, were statistically conducted. The occurrence frequencies of the two vorticity and eight directional types
269 were much higher than those of the other sixteen hybrid types, accounting for 75% of total days (Fig. 2).
270 According to the pollution intensity, three pollution types (cyclonic C, southwesterly SW and westerly W) and one
271 clean type (anticyclonic A) occurring most frequently in the NCP were selected as the studied circulation patterns.
272 It was consistent with the results of Li et al. (2020) on the relationship between pollutant concentration and
273 circulation types in northern China. Weather types with high PM2.5 concentration but occurring no more than
274 ten times, such as type CE and type CW, were not discussed in this article. The average and extreme PM2.5
275 concentrations of type C reached $77 \mu\text{g}/\text{m}^3$ and $270 \mu\text{g}/\text{m}^3$, respectively, and were much stronger than the other
276 pollution types. Clearly, the cyclonic circulation pattern was more conducive to severe pollution events. The
277 circulation of type A was the most common type, and the PM2.5 concentration was $28 \mu\text{g}/\text{m}^3$, which was the
278 lowest.

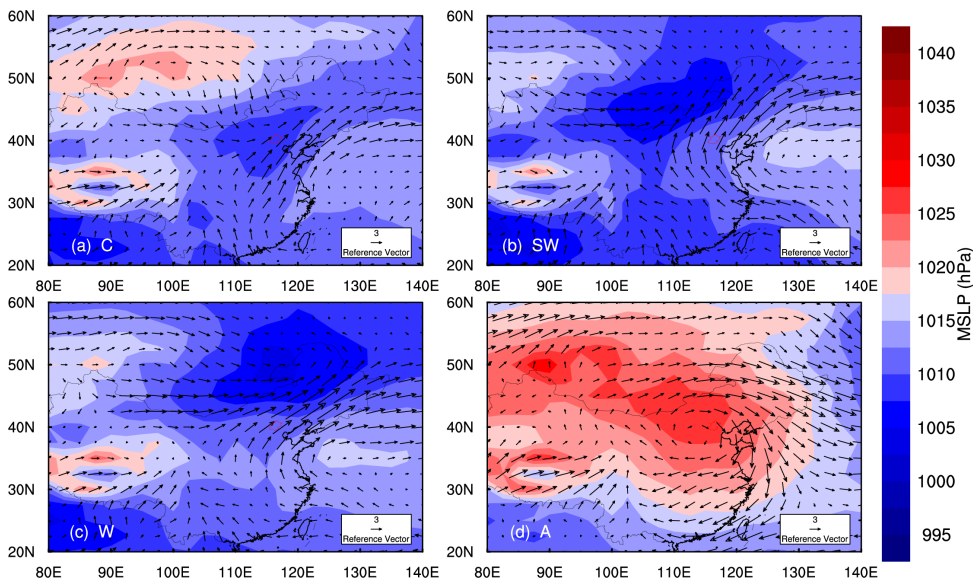
279 As shown in Fig. 3, the locations of the high and low pressures and the intensity of the wind fields at 925
280 hPa under different circulation patterns were clearly distinct. In type C, Beijing was located in the center of low
281 pressure, and the sea to the east of China was controlled by an anticyclone (Fig. 3a). Southwesterly winds
282 prevailed, flowing northward to Beijing along the periphery of the anticyclone with an average wind speed of 3
283 m/s. In type SW, Beijing lay southeast of the low pressure in Mongolia, and the high pressure over the sea was
284 significantly enhanced compared with type C (Fig. 3b). Therefore, southeasterly winds prevailed to the south of
285 Beijing and shifted southwesterly after flowing by. In type W, westerly winds were dominant and converged with
286 southwesterly flows to the north of Beijing (Fig. 3c). The mean velocity of environmental flows in type SW and
287 type W was observably larger than that in type C. In general, the mainland was mainly controlled by low pressure
288 with an anticyclone lying over the sea to the east of China in pollution types C, SW and W, and southerly flows

289 dominated at 925 hPa. By contrast, northern China in the clean type A was occupied by high pressure. Beijing was
 290 located in the center of high pressure with strong northerly winds in the lower level (Fig. 3d).

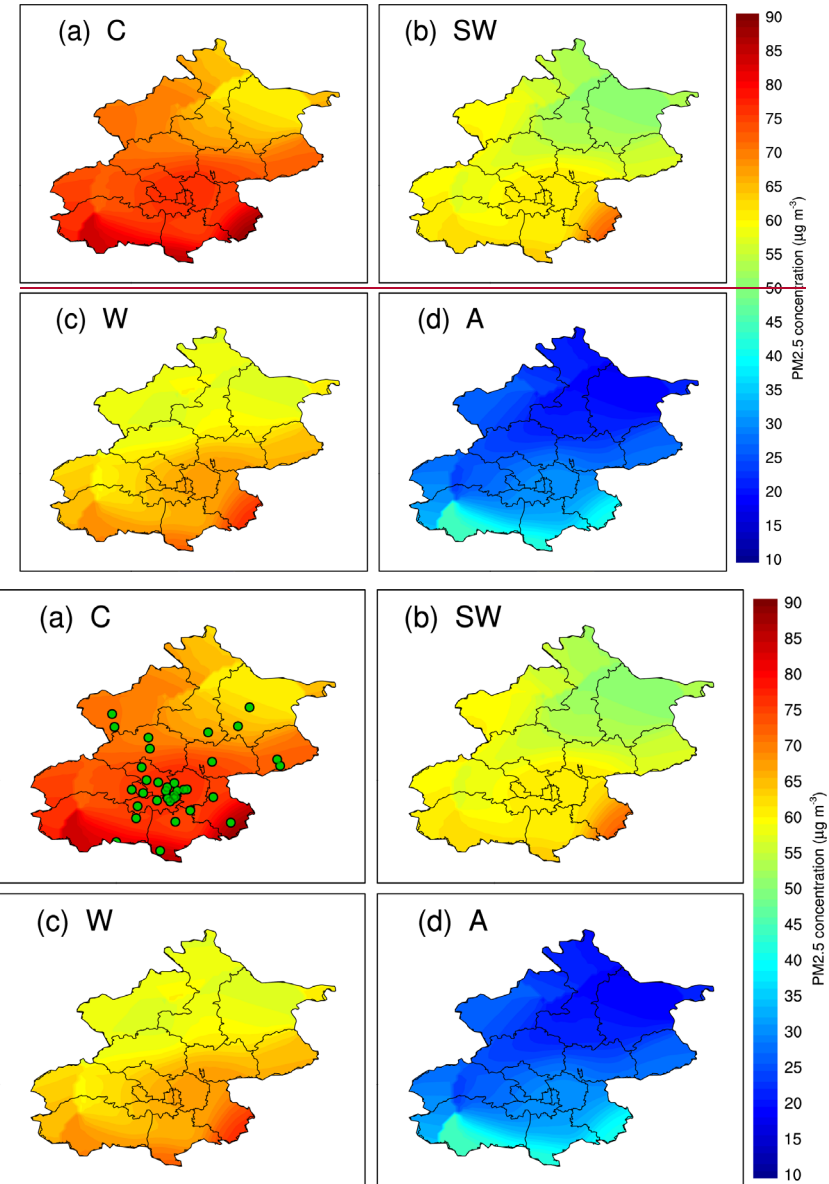
291 The pollution intensity is closely related to the large-scale weather circulations. Although the dominant
 292 synoptic patterns in different seasons vary greatly, the modulating effects on air pollution of specific circulation
 293 types in different seasons are similar (Liao et al., 2017; Li et al., 2020). The spatial distribution of PM2.5 in Beijing
 294 under pollution types C, SW, W and clean type A is shown in Fig. 4. Type C had the highest pollution level, with
 295 the PM2.5 concentration increasing from 60 $\mu\text{g}/\text{m}^3$ in the northwestern mountainous area to 90 $\mu\text{g}/\text{m}^3$ in the
 296 south-central plain area, which was significantly higher than the values for types SW and W. Type A was highly
 297 ventilated, with a PM2.5 concentration below 30 $\mu\text{g}/\text{m}^3$ in most areas. Under the influence of semibasin
 298 topography surrounded by mountains on three sides (Fig. 1b), the pollution concentrations in all weather types
 299 were characterized by a gradual decrease from southeast to northwest in Beijing.



300
 301 Fig. 2 Daily averaged PM2.5 concentration [in Olympic Center station](#) (box plots, units: $10^{-1} \mu\text{g}/\text{m}^3$) and the
 302 occurrence frequencies of 26 weather types (red dashed lines) from 2018 to 2019. The red boxes represent
 303 classical types selected for research. The black dots represent the mean values.



304
 305 Fig. 3 The daily MSLP (shaded, units: hPa) and wind fields at 925 hPa (vectors, units: m/s) for types C [\(a\)](#), SW [\(b\)](#),
 306 W [\(c\)](#) and A [\(d\)](#) from 2018 to 2019.



307
 308 Fig. 4 The averaged PM2.5 concentration (shaded, units: $10^{-1} \mu\text{g m}^{-3}$) in Beijing for types C (a), SW (b), W (c) and A (d) from 2018 to 2019. [The green dots in Fig. 4a indicate the locations of air quality monitoring sites in Beijing.](#)

310
 311 3.2 The flow field and dynamic-thermal structure of the PBL under typical weather
 312 types

313 As mentioned above, due to the special topography and geographical location in Beijing, both large-scale
 314 weather circulations and regional-scale thermal circulations have conspicuous effects on modulating pollution. In
 315 addition, the thermal and dynamic structure of the PBL also has an appreciable impact on the mixing and
 316 diffusion of pollutants. Therefore, the multiscale circulations can not only influence the pollution directly but also
 317 influence it by changing the PBL structure indirectly. To reveal the mechanisms of how the coupling effects of
 318 multiscale circulations affect the PBL structure and air pollution under different synoptic patterns, we conduct an
 319 analysis of the horizontal flow field and vertical PBL structure in depth by choosing typical cases lasting two days
 320 in the same weather type (C, SW, W and A). [The typical cases are on October 22 to 24, July 26 to 28, May 15 to 17](#)
 321 [in 2019 and December 28 to 30 in 2018 respectively.](#)

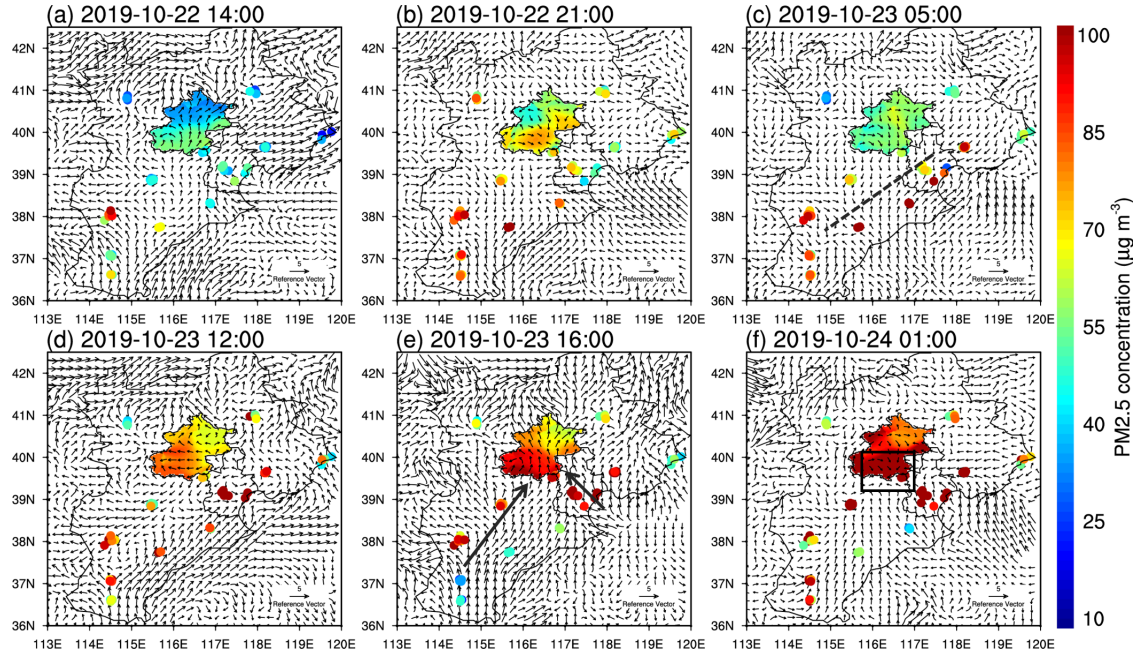
322 3.2.1 Multilayer PBL structure under type C circulation

323 The mainland was governed by low pressure under type C synoptic circulations, and the ambient winds

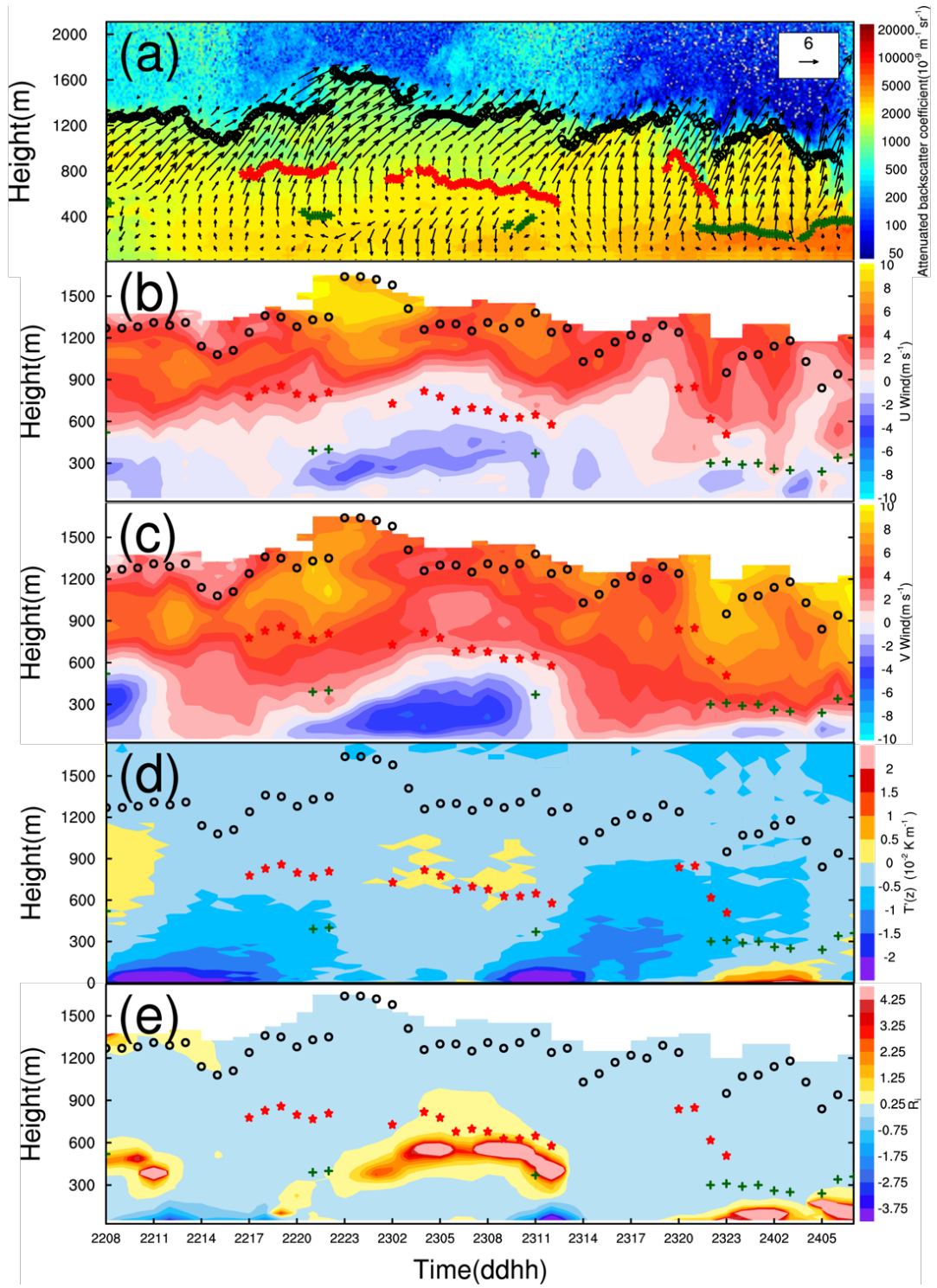
were mainly southwesterly (Fig. 3a). On the afternoon of the 22nd, the plain breezes in central Hebei, which were induced by thermal contrast between the mountain and plain, blocked weak environmental winds and the direct transportation of pollutants to Beijing (Fig. 5a). The westerly and the northerly mountain breezes began to prevail at night while the conversion from sea breeze to land breeze was not obvious (Fig. 5b). The onshore winds in the coastal area were notably larger than the northerly mountain breezes in southern Chengde (SCD), which were diverted to the west and east. The diverted easterly winds converged with the onshore winds, enhancing the easterly winds and the east pollution transport channel. Sun et al. (2019) have found that the pressure gradients between the plain and mountain areas are critical causes of the easterly winds in Beijing. Consequently, easterly winds gathered with mountain breezes and formed a pollution convergent zone. Weak environmental winds not only made the pollution channels hard to establish but also caused the pollutants to recirculate southward by strong downslope breezes further in the early morning (Fig. 5c). A mesoscale convergent belt was generated in southeastern Hebei, providing conditions for the transportation of pollutants later. At noon on the 23rd, the intensified plain winds transported high concentrations of aerosols from the right side of the convergent belt to Beijing (Fig. 5d). Large-scale environmental winds were strengthened and dominated in the afternoon (Fig. 5e), leading to the establishment of the south and east pollution transport channels and further exacerbating the air quality. On the night of the 23rd, easterly winds were observably strengthened again, joining with the downslope breezes and the ambient southerly flows (Fig. 5f). The four directional airflows formed a convergent zone that caused pollutants to accumulate dramatically in the plain areas. This convergent region that is generated by the coupling effect of large-scale circulation and regional-scale mountain breezes at night also appeared in other pollution types, as will be discussed later.

The PBL under type C circulation presented a multilayer structure without diurnal variation (Fig. 6a). The highly stable structure and weak ambient winds resulted in a higher aerosol concentration near the surface than that in the other pollution types (Fig. 4). The pollution decreased from bottom to top within the PBL and was characterized by a gradient distribution. It is consistent with previous research (Jiang et al., 2020) that the top PBL height is equal to the maximum detection range of wind Lidar. In the daytime, environmental southwesterly winds dominated within the PBL. ~~In the horizontal flow field on the night of the 22nd, meridional zonal winds from Tianjin to the southeast of Beijing turned to be easterly winds and the northerly downslope winds in Beijing were strengthened later on the night of 22nd (Fig. 5b, 5c, 6b), and the northerly downslope winds were strengthened simultaneously in the lower PBL (Fig. 5c, 6c). Inside the PBL, easterly and northerly winds were up-extended to 600 m above the ground from 20 pm on 22nd to 10 am on 23rd (Fig. 6b, 6c), thus so that the directional shear of meridional and zonal winds increased ascended considerably.~~ The shallower nocturnal PBL coincided with the zero speed zone between the upper environmental winds and lower regional-scale breezes with the largest directional shear (Fig. 6b, c). Variations of the vertical dynamic structure in the PBL drove the thermal structure to adjust. Warm air advected by large-scale southwesterly winds overlay on the cold air advected by regional-scale northeasterly breezes. Consequently, a conspicuous advective temperature inversion occurred ~~near the shallower nocturnal PBL at 08-09 am on 22nd and 00-11 am on 23, ranging~~ from 600 m to 900 m ~~above the ground~~ (Fig. 6d). ~~The Richardson number Ri away from the temperature inversion structure was less than 0.25 (turbulent region) during the night, while it increased considerably from the periphery of inversion and was larger than 1.0 (stable region) promptly. The sharp jump of Ri from the turbulent region to the stable region of inversion indicated a vertical stratified structure inside the PBL. The result suggested that the nocturnal PBL has an inhomogeneous stratification structure characterized by strong variations of Ri accompanied by inversion structure accompanied by stable stratification~~ (Fig. 6e). However, the relatively stronger northerly breezes compared to the environmental winds made the pollutants recirculate southward horizontally (Fig. 5c, 6e). Furthermore, the wind shear developed so high that the ~~dynamically~~ stable ~~region~~ stratification was above 300 m

368 and the inversion was above 600 m; the pollutants dispersed vertically to some extent consequently (Fig. 5c, 6c).
 369 Compared to the previous night, the ambient winds on the night of ~~the~~-23rd were stronger; thus, both south and
 370 east transport channels were established, along with the pollution convergent zone (Fig. 5f). The weak easterly
 371 and northerly winds were lower than 300 m (Fig. 6b, c), resulting in temperature inversion and stable
 372 stratification connected to the ground. A high concentration of pollution was accumulated in the convergent zone
 373 horizontally and trapped below the lowest PBL vertically. Thus, the PM2.5 concentration on the night of ~~the~~-23rd
 374 was significantly higher than that on ~~the~~-22nd.



375
 376 Fig. 5 The surface winds (vectors, units: $m s^{-1}$) in the NCP and PM2.5 concentration in Beijing (shaded, units: 10^{-1}
 377 $\mu g m^{-3}$), Hebei and Tianjin monitoring sites (scatter, units: $10^{-1} \mu g m^{-3}$) of different times (Local Time) for type C.
 378 The dashed line represents the convergence belt. The arrow lines represent the pollutant transport channels. The
 379 rectangle represents the convergent zone.



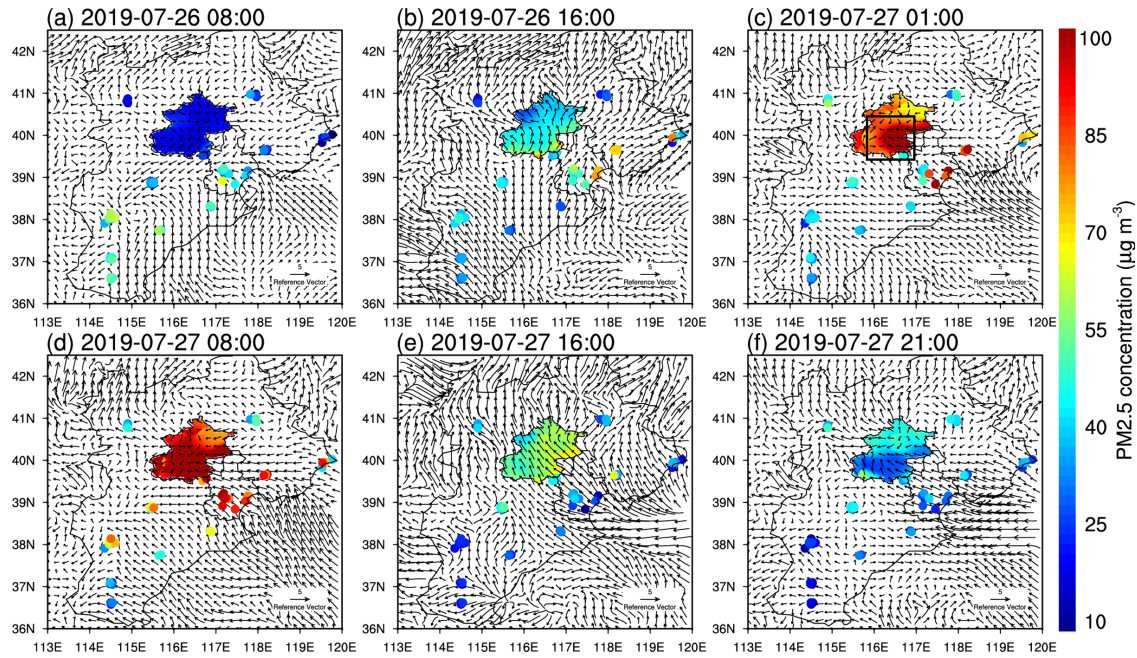
380
381 Fig. 6 Attenuated backscatter coefficient (shaded, units: $10^{-9} \text{ m}^{-1} \text{ sr}^{-1}$) [measured by ceilometer](#) and horizontal
382 winds (vectors, units: m s^{-1}) [measured by Lidar](#) (a), zonal wind [component speeds](#) (shaded, units: m s^{-1}) (b),
383 meridional wind [component speeds](#) (shaded, units: m s^{-1}) (c), gradient of temperature $T'(z)$ (shaded, units: K km^{-1})
384 [measured by MWR](#) (d), and Richardson number (shaded) (e) for type C. The green crosses, red stars and black
385 hollow dots represent the lowest, middle and top PBLH, respectively.

386 3.2.2 Mono-layer PBL structure under type SW circulation

387 Under type SW circulation, the easterly wind component increased in southeastern Hebei and the Bohai Sea,
388 and the velocity of environmental winds was appreciably higher than that in type C. (Fig. 3b). On the early

389 morning of ~~the~~-26th, mountain breezes carrying clean air masses prevailed in Beijing, and the air quality was good
390 (Fig. 7a). The basic southerly winds dominated in the Beijing-Tianjin-Hebei region in the afternoon, transporting
391 pollutants northward and causing airflow to converge in plain areas (Fig. 7b). However, pollutants were ventilated
392 horizontally by strong ambient winds and diffused vertically by the intensified turbulent mixing within the
393 growing ML, so the aerosol concentration grew slowly during the day (Fig. 8a). At night, the mountain breezes
394 were strengthened while the ambient southerly winds were weakened; hence, the pollutants were transported to
395 Beijing via the east pollution channel (Fig. 7c). Multiscale circulations of different directions joined and generated
396 a convergent zone in the plain area. Afterwards, easterly flows were further strengthened and transported
397 pollutants to Beijing continuously, the severely polluted area moved westward (Fig. 7d, 8a). In the daytime of ~~the~~
398 27th, the ambient winds prevailed again, and strong ambient winds removed pollutants by enhancing the
399 ventilation and turbulent mixing (Fig. 7e, 8a). Therefore, the PM2.5 concentration decreased instantly and the air
400 quality in the Beijing-Tianjin-Hebei region improved markedly (Fig. 7f).

401 Unlike type C, the PBL presented a monolayer structure in type SW, and the aerosol within the PBL was
402 uniformly distributed (Fig. 8a). Furthermore, the PBL had an obvious diurnal variation and the maximum
403 detection distance of wind Lidar was only consistent with the top ML in type SW. The nocturnal PBL and the
404 growing or collapsing ML were usually lower than the maximum detection distance, indicating that there were
405 residual aerosols above the PBL. In the daytime of ~~the~~-26th, southwesterly winds dominated within the PBL, and
406 the temperature lapse rate was greater than $0.5^{\circ}\text{C}/100\text{ m}$. Along with radiation reinforcing turbulent kinetic
407 energy, the PBL rose to 1200 m. Pollutants were transported to Beijing but mixed vertically (Fig. 8a), so the PM2.5
408 concentration near the surface grew slowly (Fig. 7b). On the night of ~~the~~-26th, the regional-scale circulation
409 developed upward, and the vertical wind shears between the lower regional breezes and upper environmental
410 winds were strengthened prominently (Fig. 8b, c). The warm advection overlay on the cold advection resulted in
411 advective inversion, forcing the PBL to adjust to become stable, ~~correspondingly~~ (Fig. 8d, e). Correspondingly, Ri
412 experienced an appreciable increase from the turbulent region above the PBL to the stable region of below the
413 PBL (Fig. 8e). The nocturnal PBL has a homogeneous dynamically stable structure. Similar to type C, a high
414 concentration of pollutants was trapped below the zero wind speed zone where the nocturnal PBL was located. In
415 the daytime of ~~the~~-27th, large-scale environmental winds within the PBL were strengthened greatly. The PBL
416 height was 800 m higher than that of the previous day; thus, the pollutants were advected horizontally and
417 diffused vertically (Fig. 8a). The basic southerly winds with high speed prevailed in central and southern Beijing on
418 the night of ~~the~~-27th, preventing the mountain winds from flowing southward (Fig. 7f). As a result, no vertical
419 shear of meridional winds occurred in the dynamic field (Fig. 8c) and no temperature inversion occurred in the
420 thermal field (Fig. 8d). The PM2.5 concentration was further reduced. It can be inferred that the temperature
421 inversion in type SW was generated by the vertical thermal contrast of meridional winds. When the meridional
422 winds were uniformly southerly winds within and above the PBL, the air masses in the upper layer had the same
423 thermal properties as that in the lower layer, which will reduce the vertical wind shear and destroy the stable
424 inversion structure.

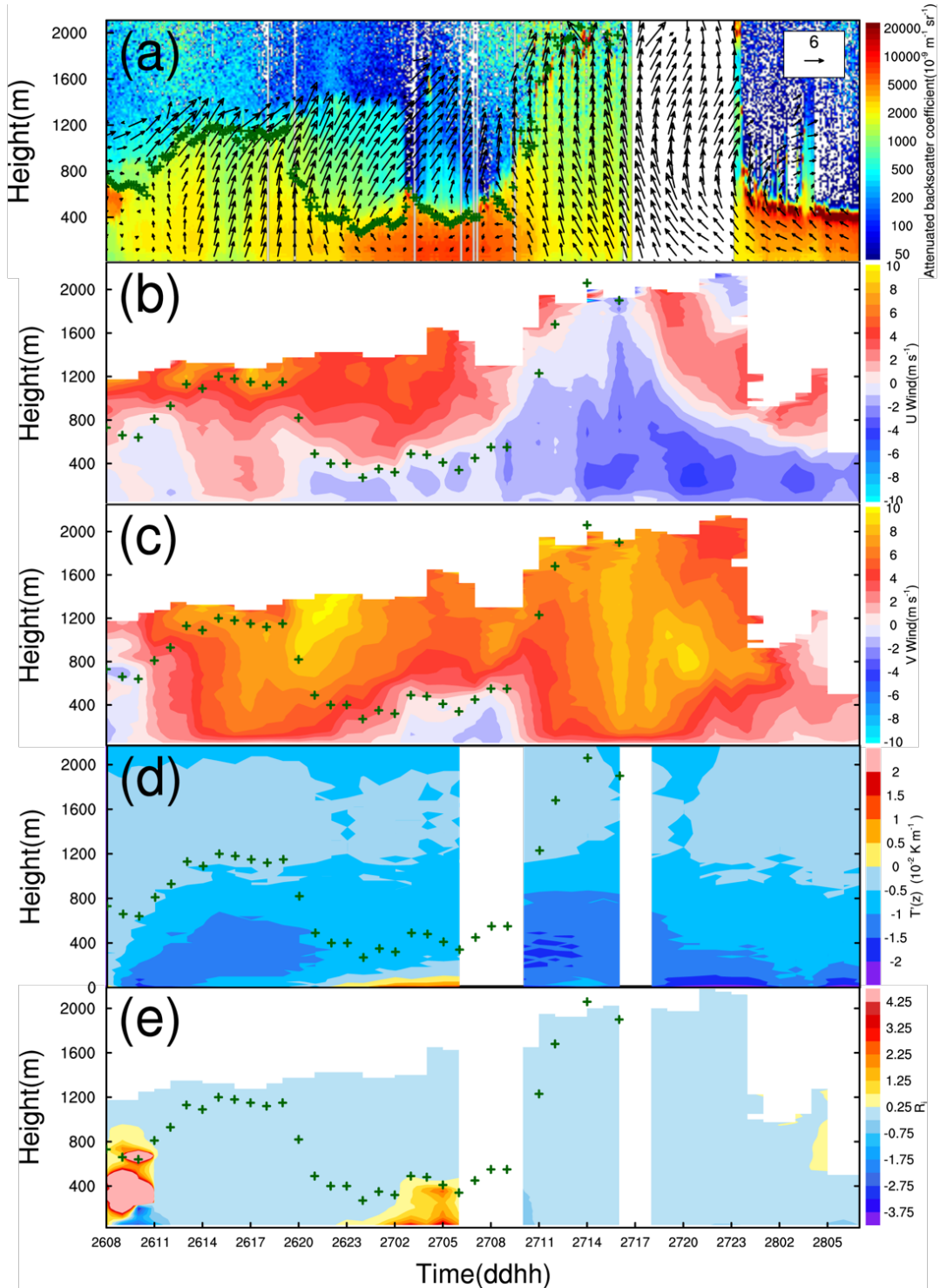


425

426 Fig. 7 The surface winds (vectors, units: m s^{-1}) in the NCP and PM2.5 concentration in Beijing (shaded, units: $10^{-1} \mu\text{g m}^{-3}$), Hebei and Tianjin monitoring sites (scatter, units: $10^{-1} \mu\text{g m}^{-3}$) of different times (Local Time) for type SW. The rectangle represents the convergent zone.

427

428



429

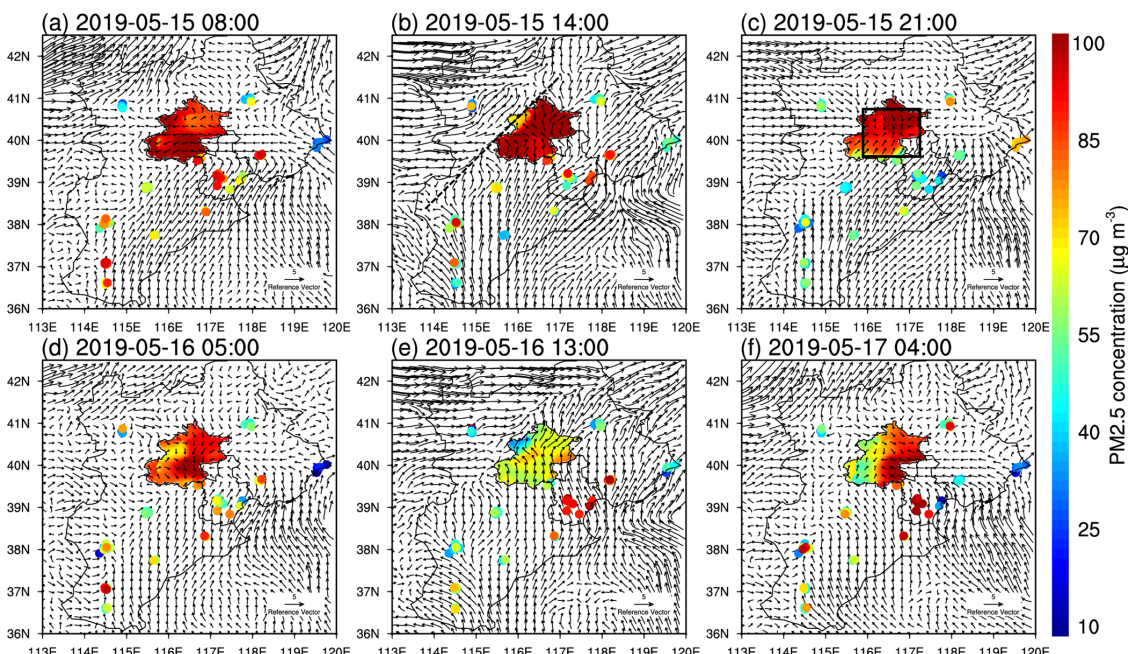
430 Fig. 8 Attenuated backscatter coefficient (shaded, units: $10^{-9} \text{ m}^{-1} \text{ sr}^{-1}$) [measured by ceilometer](#) and horizontal
 431 winds (vectors, units: m s^{-1}) [measured by Lidar](#) (a), zonal wind [component speeds](#) (shaded, units: m s^{-1}) (b),
 432 meridional wind [component speeds](#) (shaded, units: m s^{-1}) (c), gradient of temperature $T'(z)$ (shaded, units: 10^2 K km^{-1})
 433 [measured by MWR](#) (d), and Richardson number (shaded) (e) for type SW. The green crosses represent the PBLH.

434 3.2.3 Hybrid structure PBL under type W circulation

435 Under type W circulation, strong easterly winds transported a high concentration of aerosols to Beijing
 436 through the east pollution channel, and the PM2.5 concentration had already reached a high level in the early
 437 morning (Fig. 9a). Taking the mountain as the boundary, environmental westerly winds prevailed in northwestern

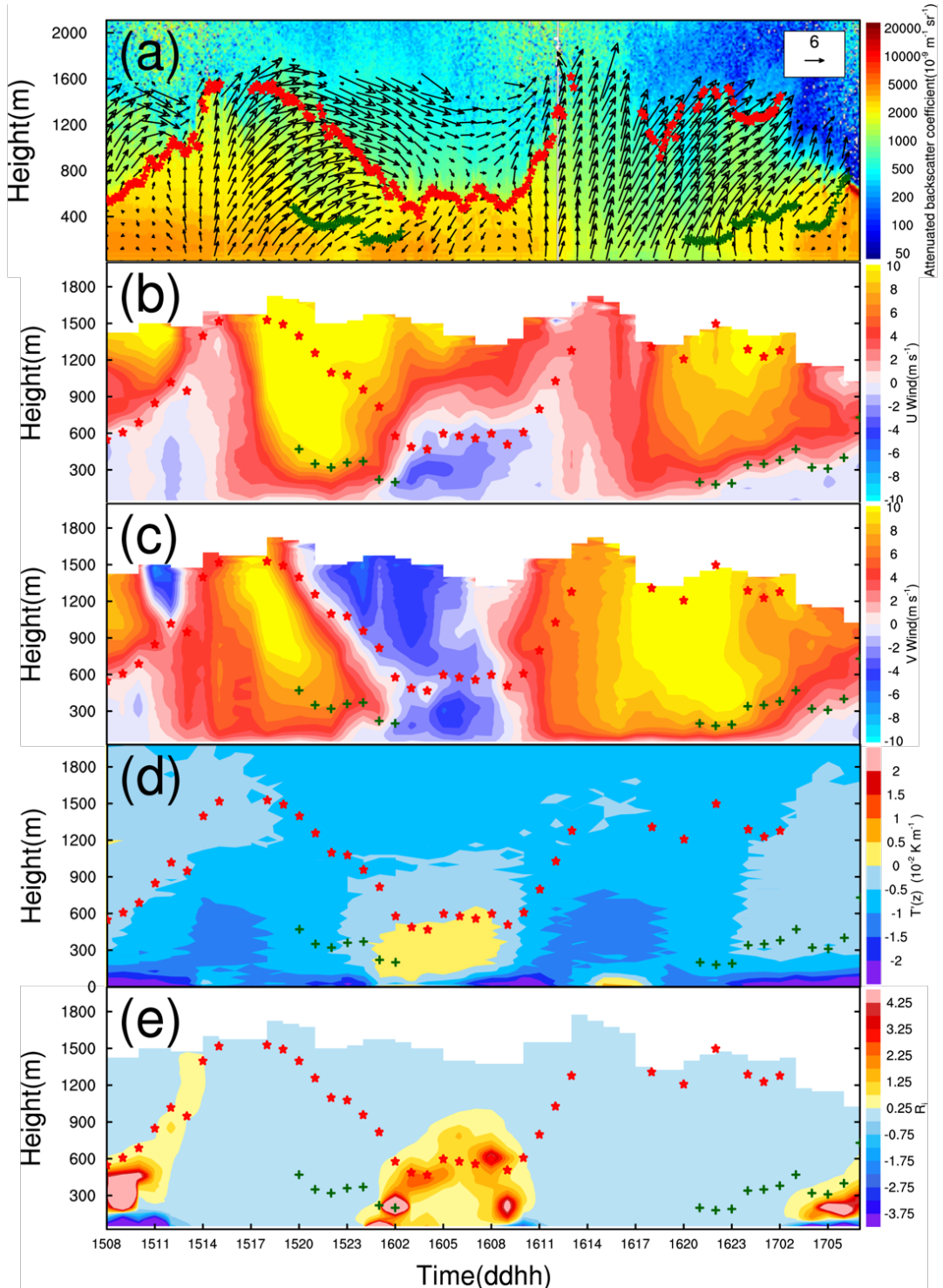
438 Hebei and southwesterly winds prevailed in southern Hebei in the afternoon. The two directional flows carried
 439 pollutants and formed a convergent belt along the western mountains (Fig. 3c, 9b). This distribution of synoptic
 440 circulations in type W was conducive to the occurrence of severe pollution around mountains. Similar to other
 441 pollution types, the ambient winds converged with region-scale mountain breezes at night, forming a convergent
 442 zone (Fig. 9c). The convergent zone moved southward later because of intensified mountain breezes (Fig. 9d). The
 443 large velocity of environmental winds leads to strong ventilation (Fig. 9e). In addition, the increasing PBL made
 444 the pollutants diluted vertically, and the air pollution was alleviated temporarily. On night of the 16th (Fig. 9f), the
 445 synergistic effects of multiscale circulations led to the convergent zone again, and pollution occurred in the
 446 easterly flows with a high PM2.5 concentration.

447 The PBL under type W circulation presented a hybrid structure, having similar characteristics of types C and
 448 SW simultaneously. Similar to type C, the aerosol concentration was characterized by a gradient distribution
 449 within the multilayer PBL (Fig. 10a). However, the PBL had an obvious diurnal variation, and the maximum
 450 detection distance of wind Lidar was only consistent with the top ML in the daytime, similar to type SW. Although
 451 the PBL height reached 1600 m in the daytime (Fig. 10a), the PM2.5 concentration at the surface did not decrease
 452 observably because of the massive pollution accumulated previously and the continuous emissions and
 453 transportation of pollutants (Fig. 9b). The mixing layer collapsed along the zero wind speed of meridional winds
 454 after sunset, and the breezes within nocturnal PBL shifted northwesterly at night (Fig. 10b, c). In type W, zonal
 455 circulation dominated. The vertical shear of zonal winds was intensified significantly at night, while the vertical
 456 shear of meridional winds diminished. Therefore, it can be assumed that the temperature inversion in type W was
 457 produced by the vertical shear of zonal winds. The thermal contrast between the upper westerly winds and the
 458 lower easterly winds produced a deep inversion layer that existed from the surface to 500 m (Fig. 10d), as well as
 459 a dynamically stable structure stratification with a depth exceeding 600 m (Fig. 10e). This is consistent with the
 460 findings of Hu et al. (2014) that westerly warm advection from the Loess Plateau was transported over the NCP
 461 and imposed a thermal inversion above the PBL. The top of the PBL was consistent with the top of the inversion
 462 and zero wind speed zone, and a high concentration of aerosols was trapped below the zero wind speed zone.



463
 464 Fig. 9 The surface winds (vectors, units: $m s^{-1}$) in the NCP and PM2.5 concentration in Beijing (shaded, units: 10^{-1}
 465 $\mu g m^{-3}$), Hebei and Tianjin monitoring sites (scatter, units: $10^{-1} \mu g m^{-3}$) of different times (Local Time) for type
 466 W. The dashed line represents the convergence belt.

467 The rectangle represents the convergent zone.



468

469 Fig. 10 Attenuated backscatter coefficient (shaded, units: $10^{-9} \text{ m}^{-1} \text{ sr}^{-1}$) [measured by ceilometer](#) and horizontal
470 winds (vectors, units: m s^{-1}) [measured by Lidar](#) (a), zonal wind [component speeds](#) (shaded, units: m s^{-1}) (b),
471 meridional wind [component speeds](#) (shaded, units: m s^{-1}) (c), gradient of temperature $T'(z)$ (shaded, units: K km^{-1})
472 [measured by MWR](#) (d), and Richardson number (shaded) (e) for type W. The green crosses and red stars represent
473 the low and top PBLH, respectively.

474 3.2.4 Strong turbulent PBL structure under clean type A circulation

475 Strikingly different from the circulations of pollution types, the mainland was under high pressure control in

476 the clean type, and northwesterly winds with a high velocity carrying clean air masses moved southward (Fig.
477 11a). Strong winds were favorable for the turbulent mixing and the vertical dispersion of pollutants. In addition,
478 the strong ventilation was beneficial to the horizontal spreading of pollutants. Due to the intense turbulent
479 mixing, the vertical wind shear and the diurnal variation of thermal field disappear, and there is no significant
480 distinct PBL structure different from the free atmosphere (Fig. 11a, b). The lapse rate of temperature was greater
481 than $1^{\circ}\text{C}/100 \text{ m}$, and Ri was less than 0.25 within the PBL (not shown). Although the aerosol concentration of the
482 clean type was far less than that of pollution types, the PBL height was only 500 m at night (Fig. 11a). Sometimes,
483 the PBL in the clean type was even lower than that of pollution types, or extended to 2-3 km swiftly because of
484 the instant upward diffusion of aerosol particulates. Unlike pollution types, the PBL height is inconsistent with the
485 maximum detection range of wind Lidar. Therefore, different circulation types should be distinguished when
486 analyzing the long-term relationships between the PBL height and pollution concentration. As shown in Fig. 12 c
487 and d, under the governing of high pressure, descending and divergent airflows of the clean type dominated the
488 whole lower and middle parts of the troposphere, and the sinking velocity was significantly higher than that of
489 pollution types. The vertical velocity changed little vertically due to the northerly winds with a large speed
490 penetrating downward. The intensity of sinking and divergence was higher at night than that in the day, with the
491 strongest divergence occurring near the surface.

492 3.3 Multiscale circulations coupling mechanism for air pollution

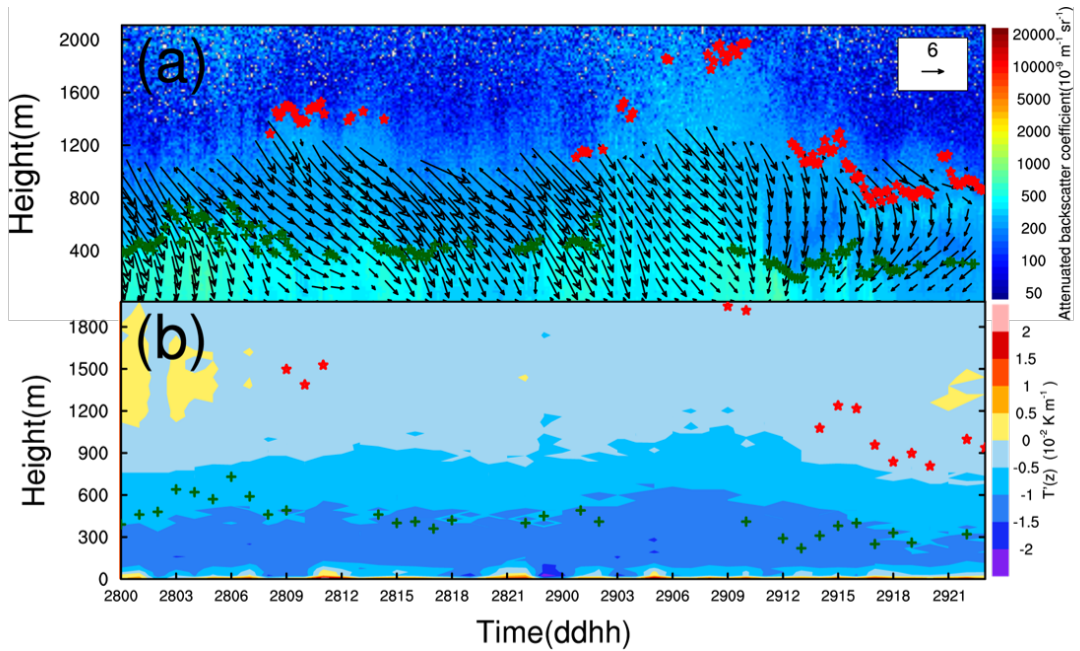
493 In addition to horizontal circulations, the vertical motion of basic airflows is also a crucial dynamic factor in
494 forming stable stratification structure during pollution episodes. The pollution types shared similar vertical
495 motion characteristics as shown in Fig. 12. The basic flows at the bottom of the troposphere is convergence and
496 the flows above it is divergence at all times of a day (Fig. 12b). In the daytime, the environmental southerly winds
497 were obstructed on three sides by mountains. Airflows slowed down or stagnated in the plain areas, forming the
498 topographic convergence. While at night the convergence was caused by the joint of environmental winds and
499 regional breezes, and the height of convergence zone reduced simultaneously with the nocturnal PBL because the
500 regional circulations developed below the shallower nocturnal PBL. Unlike the divergence field, the vertical
501 velocity in the daytime differed from that in the nighttime because of the diurnal variations of PBL structure (Fig.
502 12a). In the daytime, the thermodynamic convection and the wind speed were enhanced expressively (Fig. 8a,
503 10a), thus the intensified turbulence will help the flows to move upward and cause the pollutants close to the
504 ground to mix vertically within the PBL to some extent. In the daytime, the NCP region was controlled by a rising
505 motion at the bottom of troposphere (below about 875 hPa) below 900 hPa with a sinking motion overlaying it
506 (Fig. 12a). Correspondingly, the basic flows at the bottom of troposphere below 900 hPa presented a convergence,
507 while that above 900 hPa presented a divergence (Fig. 12b). Airflows inside the PBL converged and rose, while
508 However, the sinking and divergent flows superposed above the PBL, preventing the pollutants from moving
509 upward continuously and making it difficult for the aerosol particulates to diffuse beyond. As a consequence, the
510 pollutants accumulate slowlygradually in the daytime because of the common influences of horizontal
511 topographic blocking and vertical upward mixing with the increasing PBLML rise. However in nighttime, as the
512 thermodynamic convection weakened and the inversion structure formed, it turned to be sinking movement at
513 the bottom of the troposphere when the cold northerly regional breezes prevailed. At night, the winds presented
514 a consistent sinking motion below 500 hPa with the largest sinking velocity occurring near the surface (Fig. 12a).

515 Wu et al. (2017) found that the descending motion of synoptic circulations contributed to a reduction in the PBLH
516 by compressing the air mass. In general, the airflow of pollution types is always convergent inside the PBL with
517 the strongest convergence occurring at 950 hPa, regardless of whether it is daytime or nighttime. The height of
518 the nocturnal PBL reduced observably and simultaneously with the convergence zone; meanwhile, divergent
519 downdrafts above the PBL make it difficult for pollutants to diffuse upward (Fig. 12b). ThusTherefore, massive

520 pollutants were capped near the surface and accumulated rapidly at night under the convergent sinking motion
521 accompanied by temperature inversion structure.

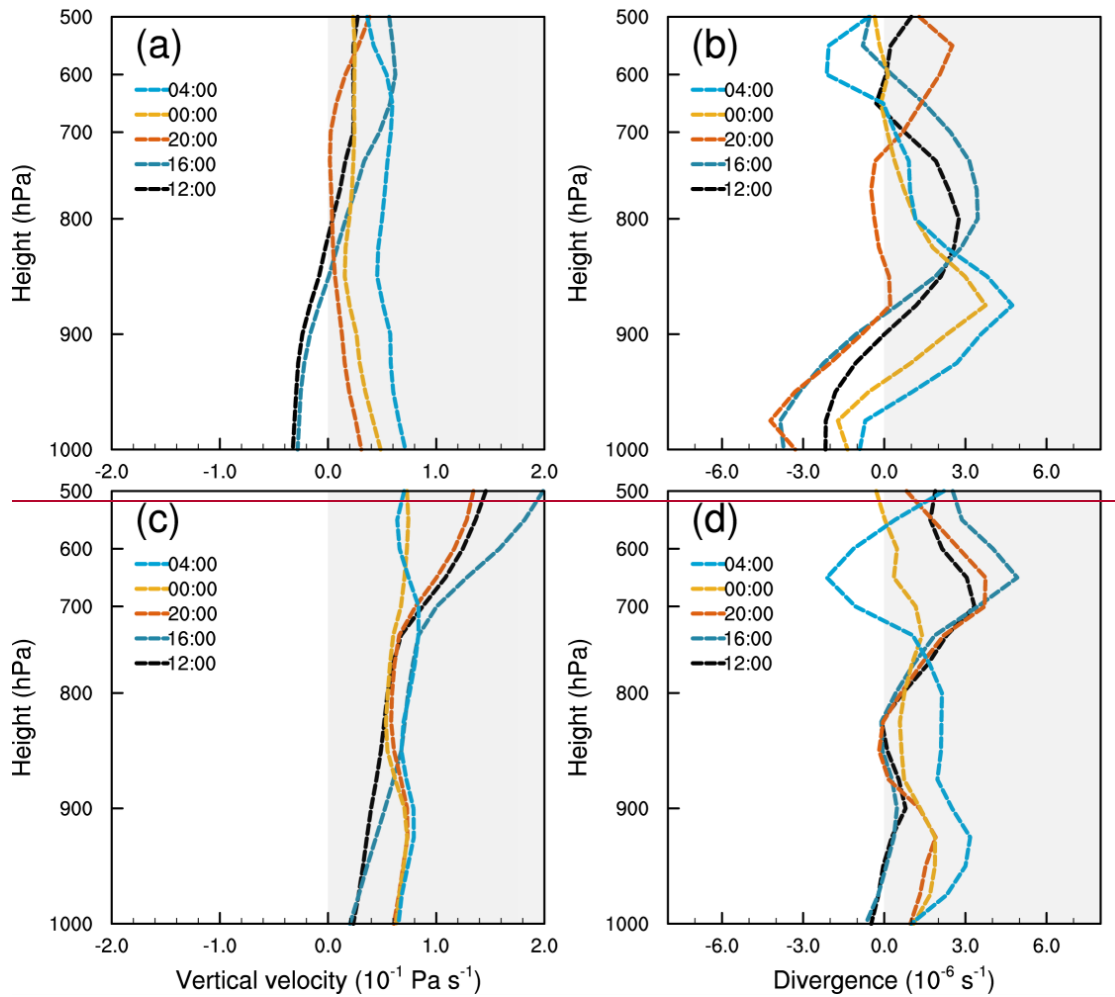
522 To sum up, different pollution patterns (C, SW and W) have similar influential mechanisms that both
523 horizontal and vertical coupling effects of the multiscale circulations have contributed to air pollution. The
524 horizontal coupling mechanism is shown in Fig. 1b. The environmental winds transport pollutants emitted from
525 southern sources to Beijing, mainly through south and east pollution channels. Large-scale environmental winds
526 and regional-scale breezes are coupled, generating a convergent zone of four directional flows horizontally and
527 aggravating the air pollution directly at night. The relative strength of winds makes the severely polluted area
528 move around horizontally from 39°N to 41°N. The schematic of Fig. 13 demonstrates that the vertical coupling
529 mechanism further influences the mixing and dispersion of pollution indirectly by changing the PBL structure. In
530 the daytime, the sinking divergent flows overlaying the rising convergent flows within the PBL inhibit the
531 continuous upward dispersion of pollutants. At night, the warm advection transported by the upper
532 environmental winds overlies the cold advection transported by the lower regional breezes, generating strong
533 directional wind shear and advective inversion, which are near the top of regional breezes. This dynamic structure
534 forces the PBL to be a stable stratification. The nocturnal PBL is located at the zero speed zone between the
535 regional-scale breezes and the environmental winds, and the relative strength of winds determines the PBL height.
536 The capping inversion cooperating with the convergent sinking motion within the PBL suppresses massive
537 pollutants below the zero speed zone.

538 ~~However, the flow field and the PBL dynamic thermal structure under different synoptic circulations vary~~
539 ~~widely with the location and intensity of high and low pressure and wind fields, resulting in differences in~~
540 ~~pollution. The multilayer PBL under type C circulation has no obvious diurnal variation. Weak ambient winds~~
541 ~~strengthen the mountain breezes observably at night. Thus, the temperature inversion and zero speed zone can~~
542 ~~reach 600 m to 900 m vertically, and the pollution convergent zone occurs in the plain areas horizontally. By~~
543 ~~contrast, the PBL under type SW circulation is a mono layer with obvious diurnal variation, reaching 2000 m in~~
544 ~~the daytime. The strong environmental winds restrain the development of regional breezes, the zero speed zone~~
545 ~~is located at 400 m and the temperature inversion is lower than 200 m at night. The inversion is generated by the~~
546 ~~vertical shear of meridional winds at night. Southerly winds within and above the PBL having the same thermal~~
547 ~~properties will diminish the vertical shear and damage the advective inversion structure. The type W circulation is~~
548 ~~governed by zonal motion and the PBL has a hybrid structure with both multiple aerosol layers and diurnal~~
549 ~~variations. The vertical comparison of zonal winds leads to a much deeper inversion and stable stratification. The~~
550 ~~pollution zone under types SW and W circulations is closer to mountainous areas because of strong ambient~~
551 ~~winds. Furthermore, strong ambient winds make the pollutants ventilate horizontally and diffuse vertically with~~
552 ~~the growing ML in the daytime.~~

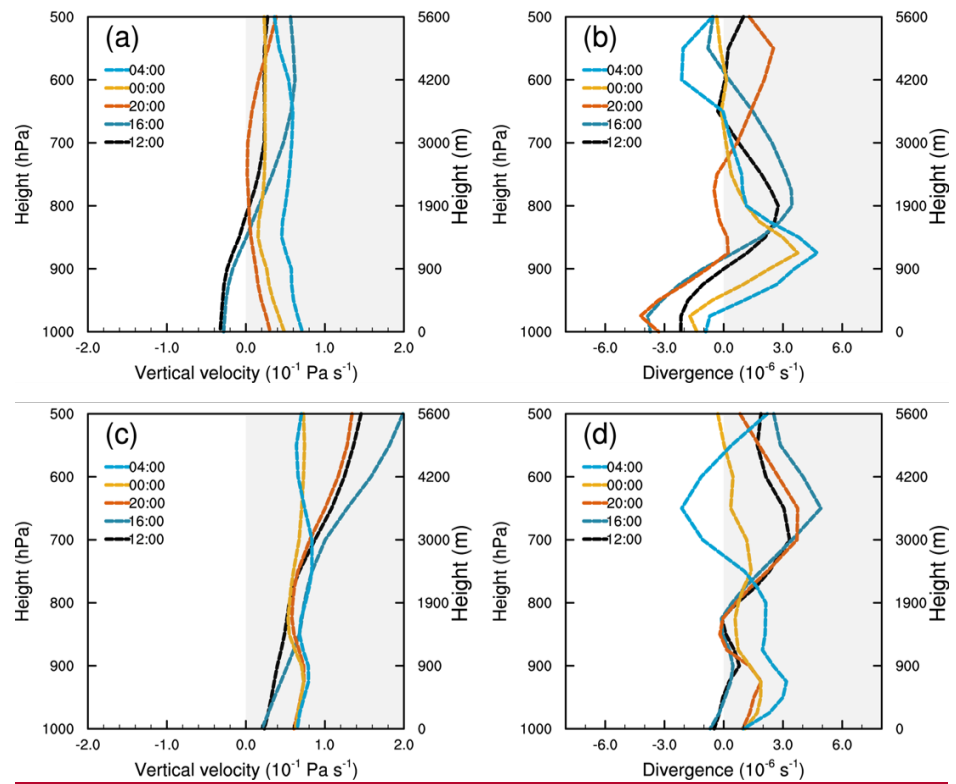


553

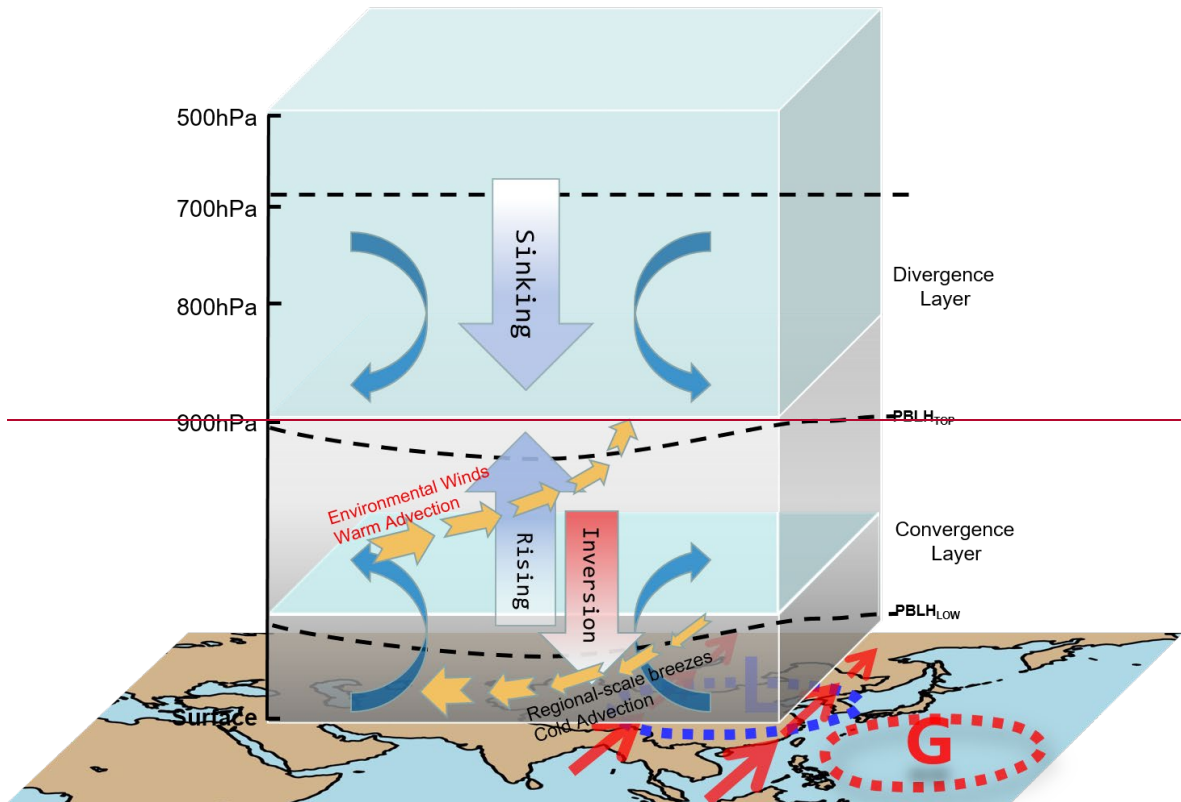
554 Fig. 11 Attenuated backscatter coefficient (shaded, units: $10^{-9} \text{ m}^{-1} \text{ sr}^{-1}$) [measured by ceilometer](#) and horizontal
 555 winds (vectors, units: m s^{-1}) [measured by Lidar](#) (a), and gradient of temperature $T'(z)$ (shaded, units: K km^{-1})
 556 [measured by MWR](#) (b) for type A. The green crosses and red stars represent the low and top PBLH, respectively.

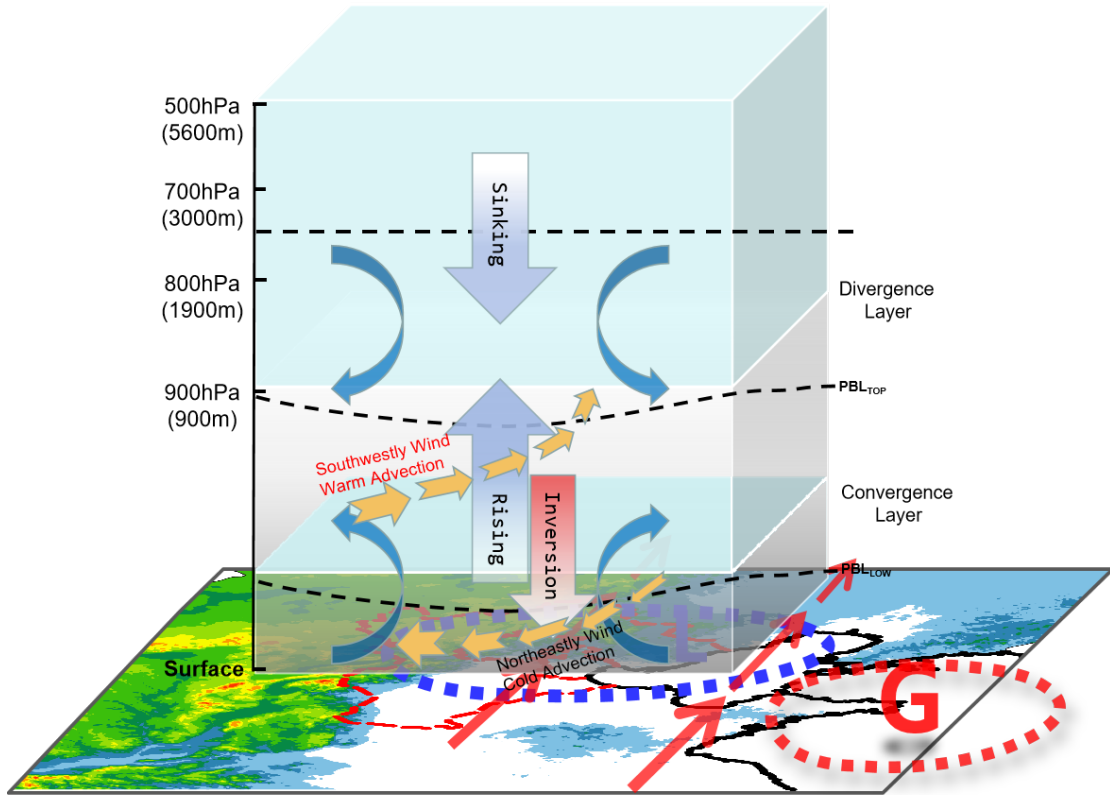


557



558
559
560 Fig. 12 The averaged vertical velocity (units: Pa s^{-1} , negative (positive) value denotes updraft (downward)
561 movement) (a, c) and divergence (units: 10^{-5} s^{-1}) (b, d) of pollution types (a, b) and the clean type (c, d) in the
562 North China Plain





564

565 Fig. 13 The schematic of vertical coupling mechanism of ~~how~~ multiscale circulations for typical pollution types;
 566 ~~affect pollution by changing~~ ~~the horizontal part is the background circulations of MSLP. The vertical part is the~~
 567 ~~PBL dynamic-thermal structure over the NCP region~~

568 4. Conclusions and Discussion

569 This paper explores the direct regulatory effect and indirect coupling effect of synoptic circulations by
 570 choosing the most frequent pollution types and clean type classified by LWT approach. The PBL dynamic-thermal
 571 structure and the severe pollution area under typical circulations types are further investigated. Results suggest
 572 that different pollution patterns have similar influential mechanisms on PBL structure and air pollution. The direct
 573 regulatory effect of synoptic circulations plays a leading role in the daytime, large-scale southerly winds dominate
 574 and are favorable for the pollution transport to NCP region and the accumulation in front of mountains in the
 575 early stage of pollution. However during the period of pollution, the relative stronger southerly winds and the
 576 increasing PBL height are adverse to the accumulation of pollutants, or even make pollutants ventilated
 577 horizontally and diluted vertically. While the indirect effect played a leading role in the nighttime by coupling
 578 mechanisms. Based on Lamb Jenkinson weather typing, the most frequent typical pollution types and clean type
 579 were chosen to explore the flow field and the PBL structure under different synoptic patterns. In addition, the
 580 horizontal and vertical coupling mechanisms of multiscale circulations, which aggravated pollution synergistically,
 581 were further revealed. The results show that different pollution patterns have similar influential mechanisms for
 582 air pollution. The coexisting multiscale circulations at night, on the one hand, affect the pollution directly via the
 583 horizontal coupling effect, which produces a pollution convergent zone of different direction winds. The relative
 584 strength of winds makes the severely polluted area move around horizontally between 39°N and 41°N. On the
 585 other hand, the multiscale circulations regulate the mixing and diffusion of pollutants indirectly by the vertical
 586 coupling effect, which changes the PBL dynamic and thermal structure. Vertical shear between the ambient winds
 587 and regional-scale breezes leads to advection inversion structure with strong variations of Ri. The nocturnal

588 shallower PBL is consistent with the zero velocity zone, where massive pollutants were suppressed below, and the
589 relative strength of winds determines the PBL height. Vertical shear between the ambient winds and
590 regional scale breezes leads to advective inversion and stable stratification, and the relative strength of winds
591 determines the PBL height. Massive pollutants were suppressed below the zero speed zone by the capping
592 inversion and the convergent sinking motion within the PBL.

593 The multilayer PBL under type C circulation has no diurnal variation. Weak ambient winds strengthen the
594 mountain breezes observably at night, as a result the vertical shear and temperature inversion can reach 600m
595 and 900 m respectively. An inhomogeneous stratification with sharp jump of Ri is formed from the periphery of
596 inversion. The severe polluted area was located to the south of Beijing. The mono-layer PBL under southwesterly
597 circulation with obvious diurnal variation can reach 2000 m in the daytime. Strong environmental winds restrain
598 the development of regional breezes at night, the zero speed zone is located at 400 m and the inversion
599 generated by the vertical shear of meridional winds is lower than 200 m. Southerly winds within and above the
600 PBL having the same thermal properties will diminish the vertical shear and damage the advective inversion
601 structure. The PBL under westerly circulation has a hybrid structure with both multiple aerosol layers and diurnal
602 variation. The inversion is generated by the vertical shear of zonal winds. The polluted areas under southwesterly
603 and westerly circulations are located more northerly. Clean and strong north winds are dominated under
604 anticyclone circulation, the vertical shear and the diurnal variation of thermal field disappear and there is no
605 distinct PBL structure.

606 This study suggests that synoptic-scale circulations or the regional-scale circulations don't influence the PBL
607 structure and air pollution separately but by the synergistic ways instead. The new knowledge of the coupling
608 mechanism of multiscale circulations has appreciable implications for deepening the understanding of
609 cooperation of influential factors in severe pollution processes in the background of unique topography. The new
610 findings about the PBL dynamic-thermal structure and the distribution of pollution provide a reference for
611 forecasting the severe pollution area under the most frequent synoptic circulation types in Beijing. Although the
612 essential impacts of synoptic-scale and regional-scale circulations on PBL dynamic-thermal structure are
613 emphasized in the paper, the feedback impact of aerosols should not be neglect either when investigating the PBL
614 structure and air pollution. The distinctions of the flow field and PBL dynamic thermal structure result in the
615 differences of horizontal and vertical pollution, respectively. Based on the fact that both the flow field and PBL
616 structure are dominated by synoptic circulations, the atmospheric environmental capacity (AEC) may vary day by
617 day following the changes in the circulations. Especially when the pollution and meteorological conditions are
618 layered within the PBL, the traditional calculation approach of AEC, which treats the PBL as a uniform and
619 homogenous layer, is no longer applicable. Future work on the quantitative relationships between the PBL
620 structure and air pollution under different weather patterns still needs to be performed. The algorithm of AEC
621 under synoptic circulations with a multilayer PBL, such as cyclonic type circulation, also needs to be improved.

622 Data availability

623 The hourly ground level PM2.5 concentration data can be obtained from the National Urban Air Quality
624 Real-time Publishing Platform (<http://106.37.208.233:20035/>). Other data used in this study can be acquired upon
625 request to the corresponding author.

626 Competing interests

627 The authors declare that they have no known competing financial interests or personal relationships that
628 could have appeared to influence the work reported in this paper.

629 Author contribution

JY performed the idea, methodology, data processing, visualization and writing. XJ provided writing guidance and funding, revised and polished the paper. WY performed supervision. TG contributed to observation data and discussions of results. ZY provided the research data and method. JD, ZD, WM and DL participated in the discussions. WL, WT and WF provided resources. All the authors have made substantial contributions to this article. XJ designed the study. JY, WY, TG, JD, ZD, WM, DL, WL, WT, WF contributed to observation data, provided experimental assistance and analyzed methodology. JY and XJ wrote the paper with inputs from all the other authors.

Acknowledgments

This study was supported by [the National Key Research and Development Program of China](#) [the Ministry of Science and Technology of China](#) (grant number 2016YFC0202001) and the [Chinese Academy of Sciences CAS](#) Strategic Priority Research Program (XDA23020301).

References

Aitken, M. L., Rhodes, M. E., and Lundquist, J. K.: Performance of a Wind-Profiling Lidar in the Region of Wind Turbine Rotor Disks, *Journal of Atmospheric and Oceanic Technology*, 29, 347-355, 2012.

Banakh, V. A., Smalikho, I. N., and Falits, A. V.: Wind-Temperature Regime and Wind Turbulence in a Stable Boundary Layer of the Atmosphere: Case Study, *Remote Sensing*, 12, 955, 2020.

Bei, N., Zhao, L., Wu, J., Li, X., Feng, T., and Li, G.: Impacts of sea-land and mountain-valley circulations on the air pollution in Beijing-Tianjin-Hebei (BTH): A case study, *Environmental Pollution*, 234, 429-438, 2018.

Chen, Y., Zhao, C., Zhang, Q., Deng, Z., Huang, M., and Ma, X.: Aircraft study of Mountain Chimney Effect of Beijing, China, *Journal of Geophysical Research-Atmospheres*, 114, 2009.

Cheng, Z., Luo, L., Wang, S., Wang, Y., Sharma, S., Shimadera, H., Wang, X., Bressi, M., de Miranda, R. M., Jiang, J., Zhou, W., Fajardo, O., Yan, N., and Hao, J.: Status and characteristics of ambient PM2.5 pollution in global megacities, *Environment International*, 89-90, 212-221, 2016.

Dai, L., Xin, J., Zuo, H., Ma, Y., Zhang, L., Wu, X., Ma, Y., Jia, D., and Wu, F.: Multilevel Validation of Doppler Wind Lidar by the 325 m Meteorological Tower in the Planetary Boundary Layer of Beijing, *Atmosphere*, 11, 1051, 2020.

Ding, A. J., Huang, X., Nie, W., Sun, J. N., Kerminen, V. M., Petaja, T., Su, H., Cheng, Y. F., Yang, X. Q., Wang, M. H., Chi, X. G., Wang, J. P., Virkkula, A., Guo, W. D., Yuan, J., Wang, S. Y., Zhang, R. J., Wu, Y. F., Song, Y., Zhu, T., Zilitinkevich, S., Kulmala, M., and Fu, C. B.: Enhanced haze pollution by black carbon in megacities in China, *Geophysical Research Letters*, 43, 2873-2879, 2016.

Fu, G. Q., Xu, W. Y., Yang, R. F., Li, J. B., and Zhao, C. S.: The distribution and trends of fog and haze in the North China Plain over the past 30 years, *Atmospheric Chemistry and Physics*, 14, 11949-11958, 2014.

Gryning, S.-E., Floors, R., Pena, A., Batchvarova, E., and Bruemmer, B.: Weibull Wind-Speed Distribution Parameters Derived from a Combination of Wind-Lidar and Tall-Mast Measurements Over Land, Coastal and Marine Sites, *Boundary-Layer Meteorology*, 159, 329-348, 2016.

Hu, X.-M., Ma, Z., Lin, W., Zhang, H., Hu, J., Wang, Y., Xu, X., Fuentes, J. D., and Xue, M.: Impact of the Loess Plateau on the atmospheric boundary layer structure and air quality in the North China Plain: A case study, *Science of the Total Environment*, 499, 228-237, 2014.

Huang, M., Gao, Z., Miao, S., and Xu, X.: Characteristics of sea breezes over the Jiangsu coastal area, China, *International Journal of Climatology*, 36, 3908-3916, 2016.

Jenkinson, A. F., and Collison, F. P.: An initial climatology of gales over the North Sea, *Synoptic climatology branch memorandum*, 62, 18, 1977.

672 Jiang, Y., Xin, J., Zhao, D., Jia, D., Tang, G., Quan, J., Wang, M., and Dai, L.: Analysis of differences between
673 thermodynamic and material boundary layer structure: Comparison of detection by ceilometer and
674 microwave radiometer, *Atmospheric Research*, 248, 105179, 2021.

675 Kotthaus, S., and Grimmond, C. S. B.: Atmospheric boundary-layer characteristics from ceilometer measurements.
676 Part 1: A new method to track mixed layer height and classify clouds, *Quarterly Journal of the Royal
677 Meteorological Society*, 144, 1525-1538, 2018.

678 Lamb, H. H., and Hh, L.: British Isles weather types and a register of the daily sequence of circulation patterns
679 1861-1971, 1972.

680 Li, L.-j., Ying, W., Zhang, Q., Tong, Y. U., Yue, Z., and Jun, J. I. N.: Spatial distribution of aerosol pollution based on
681 MODIS data over Beijing, China, *Journal of Environmental Sciences*, 19, 955-960, 2007.

682 Li, M., Wang, L., Liu, J., Gao, W., Song, T., Sun, Y., Li, L., Li, X., Wang, Y., Liu, L., Daellenbach, K. R., Paasonen, P. J.,
683 Kerminen, V.-M., Kulmala, M., and Wang, Y.: Exploring the regional pollution characteristics and
684 meteorological formation mechanism of PM2.5 in North China during 2013-2017, *Environment International*,
685 134, 105283, 2020.

686 Li, X., Ma, Y., Wei, W., Zhang, Y., Liu, N., Hong, Y., and Wang, Y.: Vertical Distribution of Particulate Matter and its
687 Relationship with Planetary Boundary Layer Structure in Shenyang, Northeast China, *Aerosol and Air Quality
688 Research*, 19, 2464-2476, 2019.

689 Li, Z., Guo, J., Ding, A., Liao, H., Liu, J., Sun, Y., Wang, T., Xue, H., Zhang, H., and Zhu, B.: Aerosol and
690 boundary-layer interactions and impact on air quality, *National Science Review*, 4, 810-833, 2017.

691 Liao, Z., Gao, M., Sun, J., and Fan, S.: The impact of synoptic circulation on air quality and pollution-related human
692 health in the Yangtze River Delta region, *Science of the Total Environment*, 607, 838-846, 2017.

693 Liu, S., Liu, Z., Li, J., Wang, Y., Ma, Y., Sheng, L., Liu, H., Liang, F., Xin, G., and Wang, J.: Numerical simulation for the
694 coupling effect of local atmospheric circulations over the area of Beijing, Tianjin and Hebei Province, *Science
695 in China Series D-Earth Sciences*, 52, 382-392, 2009.

696 Lou, M., Guo, J., Wang, L., Xu, H., Chen, D., Miao, Y., Lv, Y., Li, Y., Guo, X., Ma, S., and Li, J.: On the Relationship
697 Between Aerosol and Boundary Layer Height in Summer in China Under Different Thermodynamic
698 Conditions, *Earth and Space Science*, 6, 887-901, 2019.

699 Miao, Y., Guo, J., Liu, S., Liu, H., Li, Z., Zhang, W., and Zhai, P.: Classification of summertime synoptic patterns in
700 Beijing and their associations with boundary layer structure affecting aerosol pollution, *Atmospheric
701 Chemistry and Physics*, 17, 3097-3110, 2017.

702 Miao, Y., Hu, X.-M., Liu, S., Qian, T., Xue, M., Zheng, Y., and Wang, S.: Seasonal variation of local atmospheric
703 circulations and boundary layer structure in the Beijing-Tianjin-Hebei region and implications for air quality,
704 *Journal of Advances in Modeling Earth Systems*, 7, 1602-1626, 2015a.

705 Miao, Y., Liu, S., Zheng, Y., Wang, S., Chen, B., Zheng, H., and Zhao, J.: Numerical study of the effects of local
706 atmospheric circulations on a pollution event over Beijing-Tianjin-Hebei, China, *Journal of Environmental
707 Sciences*, 30, 9-20, 2015b.

708 Muenkel, C., Eresmaa, N., Rasanen, J., and Karppinen, A.: Retrieval of mixing height and dust concentration with
709 lidar ceilometer, *Boundary-Layer Meteorology*, 124, 117-128, 2007.

710 O'Connor, E. J., Illingworth, A. J., Brooks, I. M., Westbrook, C. D., Hogan, R. J., Davies, F., and Brooks, B. J.: A
711 Method for Estimating the Turbulent Kinetic Energy Dissipation Rate from a Vertically Pointing Doppler Lidar,
712 and Independent Evaluation from Balloon-Borne In Situ Measurements, *Journal of Atmospheric and Oceanic
713 Technology*, 27, 1652-1664, 2010.

714 Petaja, T., Jarvi, L., Kerminen, V. M., Ding, A. J., Sun, J. N., Nie, W., Kujansuu, J., Virkkula, A., Yang, X. Q., Fu, C. B.,
715 Zilitinkevich, S., and Kulmala, M.: Enhanced air pollution via aerosol-boundary layer feedback in China,

716 [Scientific Reports, 6, 18998, 2016.](#)

717 [Quan, J., Tie, X., Zhang, Q., Liu, Q., Li, X., Gao, Y., and Zhao, D.: Characteristics of heavy aerosol pollution during](#)

718 [the 2012-2013 winter in Beijing, China, Atmospheric Environment, 88, 83-89, 2014.](#)

719 [Song, C., Wu, L., Xie, Y., He, J., Chen, X., Wang, T., Lin, Y., Jin, T., Wang, A., and Liu, Y.: Air pollution in China: Status](#)

720 [and spatiotemporal variations, Environmental pollution, 227, 334-347, 2017.](#)

721 [Steyn, D. G., Baldi, M., and Hoff, R. M.: The detection of mixed layer depth and entrainment zone thickness from](#)

722 [lidar backscatter profiles, Journal of Atmospheric and Oceanic Technology, 16, 953-959, 1999.](#)

723 [Stull, R. B.: An Introduction to Boundary Layer Meteorology, Kluwer Academic Publishers, Dordrecht, 1988.](#)

724 [Sun, Z.-b., Wang, H., Guo, C., Wu, J., Cheng, T., and Li, Z.-m.: Barrier effect of terrain on cold air and return flow of](#)

725 [dust air masses, Atmospheric Research, 220, 81-91, 2019.](#)

726 [Suomi, I., Gryning, S.-E., O'Connor, E. J., and Vihma, T.: Methodology for obtaining wind gusts using Doppler lidar,](#)

727 [Quarterly Journal of the Royal Meteorological Society, 143, 2061-2072, 2017.](#)

728 [Tai, A. P. K., Mickley, L. J., and Jacob, D. J.: Correlations between fine particulate matter \(PM2. 5\) and](#)

729 [meteorological variables in the United States: Implications for the sensitivity of PM2.5 to climate change,](#)

730 [Atmospheric Environment, 44, 3976-3984, 2010.](#)

731 [Tang, G., Zhu, X., Hu, B., Xin, J., Wang, L., Muenkel, C., Mao, G., and Wang, Y.: Impact of emission controls on air](#)

732 [quality in Beijing during APEC 2014: lidar ceilometer observations, Atmospheric Chemistry and Physics, 15,](#)

733 [12667-12680, 2015.](#)

734 [Trigo, R. M., and DaCamara, C. C.: Circulation weather types and their influence on the precipitation regime in](#)

735 [Portugal, International Journal of Climatology, 20, 1559-1581, 2000.](#)

736 [Tsaknakis, G., Papayannis, A., Kokkalis, P., Amiridis, V., Kambezidis, H. D., Mamouri, R. E., Georgouassis, G., and](#)

737 [Avdikos, G.: Inter-comparison of lidar and ceilometer retrievals for aerosol and Planetary Boundary Layer](#)

738 [profiling over Athens, Greece, Atmospheric Measurement Techniques, 4, 1261-1273, 2011.](#)

739 [Wang, X., Dickinson, R. E., Su, L., Zhou, C., and Wang, K.: PM2.5 POLLUTION IN CHINA AND HOW IT HAS BEEN](#)

740 [EXACERBATED BY TERRAIN AND METEOROLOGICAL CONDITIONS, Bulletin of the American Meteorological](#)

741 [Society, 99, 105-120, 2018.](#)

742 [Wu, P., Ding, Y., and Liu, Y.: Atmospheric circulation and dynamic mechanism for persistent haze events in the](#)

743 [Beijing-Tianjin-Hebei region, Advances in Atmospheric Sciences, 34, 429-440, 2017.](#)

744 [Xu, T., Song, Y., Liu, M., Cai, X., Zhang, H., Guo, J., and Zhu, T.: Temperature inversions in severe polluted days](#)

745 [derived from radiosonde data in North China from 2011 to 2016, Science of the Total Environment, 647,](#)

746 [1011-1020, 2019.](#)

747 [Ye, X., Song, Y., Cai, X., and Zhang, H.: Study on the synoptic flow patterns and boundary layer process of the](#)

748 [severe haze events over the North China Plain in January 2013, Atmospheric Environment, 124, 129-145,](#)

749 [2016.](#)

750 [Yu, B., Zhu, B., Dou, J., Zhang, W., and Hu, D.: Classification of air pollution synoptic patterns and air pollutants](#)

751 [transport/purification effect by cold front over Hangzhou, China Environmental Science, 37, 452-459, 2017.](#)

752 [Zhang, R.: Warming boosts air pollution, Nature Climate Change, 7, 238-239, 2017.](#)

753 [Zhang, Y., Ding, A., Mao, H., Nie, W., Zhou, D., Liu, L., Huang, X., and Fu, C.: Impact of synoptic weather patterns](#)

754 [and inter-decadal climate variability on air quality in the North China Plain during 1980-2013, Atmospheric](#)

755 [Environment, 124, 119-128, 2016.](#)

756 [Zhang, Y., Guo, J., Yang, Y., Wang, Y., and Yim, S. H. L.: Vertical Wind Shear Modulates Particulate Matter Pollutions:](#)

757 [A Perspective from Radar Wind Profiler Observations in Beijing, China, Remote Sensing, 12, 546, 2020.](#)

758 [Zhao, D., Xin, J., Gong, C., Quan, J., Liu, G., Zhao, W., Wang, Y., Liu, Z., and Song, T.: The formation mechanism of](#)

759 [air pollution episodes in Beijing city: Insights into the measured feedback between aerosol radiative forcing](#)

760 and the atmospheric boundary layer stability, *Science of the Total Environment*, 692, 371-381, 2019.
761 Zheng, X. Y., Fu, Y. F., Yang, Y. J., and Liu, G. S.: Impact of atmospheric circulations on aerosol distributions in
762 autumn over eastern China: observational evidence, *Atmospheric Chemistry and Physics*, 15, 12115-12138,
763 2015.